Optimized Substrate Positioning Enables Switches in C–H Cleavage Site and Reaction Outcome in the Hydroxylation-Epoxidation Sequence Catalyzed by Hyoscyamine 6β-Hydroxylase

Keywords: Scopolamine, Epoxide, Iron, 2-Oxoglutarate, Oxygenase

Eliott S. Wenger,[1,3] Ryan J. Martinie,[1,4] Richiro Ushimaru,[5] Christopher J. Pollock,[1,6] Debangsu Sil,[1,7] Aaron Li,[2,8] Nhi Hoang,[2,9] Gavin M. Palowitch,[2,10] Brandt P. Graham,[1] Irene Schaperdoth,[1,11] Evan J. Burke,[1] Ailiena Maggiolo,[1,12] Wei-Chen Chang,[13] Benjamin D. Allen,[2,14] Carsten Krebs,[1,2,*] Alexey Silakov,[1,*] Amie K. Boal,[1,2,*] J. Martin Bollinger, Jr.[1,2,*]

[1]Department of Chemistry and [2]Department of Biochemistry and Molecular Biology, The Pennsylvania State University, University Park, PA 16802, United States

[3]Department of Chemistry, University of Pennsylvania, Philadelphia, PA 19104, United States

[4]Present address: Hamilton College, 198 College Hill Road, Clinton, NY 13323, United States

[5]Graduate School of Pharmaceutical Sciences, The University of Tokyo, Tokyo 113-8657, Japan

[6]Present address: Cornell High Energy Synchrotron Source, Wilson Laboratory, Cornell University, Ithaca, NY 14853, United States

[7]Present address: Department of Chemistry, Indian Institute of Science Education & Research-Pune, Pune 411008, Maharashtra, India

[8]Present address: Spark Therapeutics, 3025 Market Street, Philadelphia, PA 19104, United States

[9]Present address: Pfizer, 401 N Middletown Rd, Pearl River, NY 10965, United States

[10]Present address: BioNTech US, 40 Erie Street, Cambridge, MA 02139, United States

[11]Present address: Thayer School of Engineering at Dartmouth, 15 Thayer Drive, Hanover, NH 03755, United States

[12]Present address: SLAC National Accelerator Laboratory, Menlo Park, CA 94025, United States

[13]Present address: Department of Chemistry, North Carolina State University, Raleigh, NC 27607, United States

[14]Present address: Tandem Repeat Technologies, Inc., 110 Canal Street, 4th Floor, Lowell MA 01852, United States

Table of Contents Figure

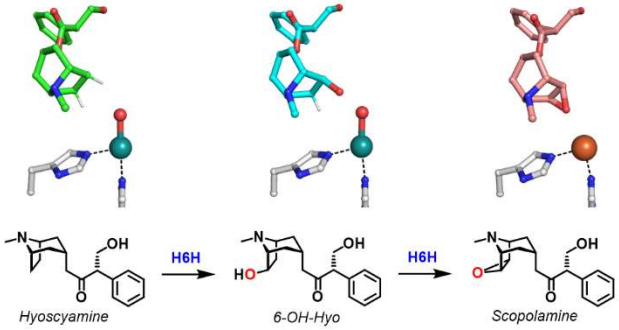

Abstract

Hyoscyamine 6β-hydroxylase (H6H) is an Fe(II)- and 2-oxoglutarate-dependent (Fe/2OG) oxygenase that catalyzes the last two steps in the biosynthesis of scopolamine, a prolifically administered anti-nausea drug. After its namesake first reaction, H6H couples the newly installed C6-bonded oxygen to C7 to form the epoxide of scopolamine. Oxoiron(IV) (ferryl) intermediates initiate both reactions by cleaving C–H bonds, but it remains unclear how the enzyme switches target site and promotes (C6)O–C7 coupling in preference to C7 hydroxylation in the second step. In one possible epoxidation mechanism, the C6 oxygen would – analogously to mechanisms proposed for the Fe/2OG halogenases and, in a parallel study, *N*-acetylnorloline synthase (LolO) – coordinate as alkoxide to the C7–H-cleaving ferryl intermediate to enable alkoxyl coupling to the ensuing C7 radical. Here we provide structural and kinetic evidence that H6H instead exploits the distinct spatial dependencies of competitive C–H-cleavage (C6 vs C7) and C–O-coupling (oxygen rebound vs cyclization) steps to promote the two-step sequence without substrate coordination or repositioning for the epoxidation step. Structural comparisons of ferryl-mimicking vanadyl complexes of wild-type H6H and a variant that preferentially 7-hydroxylates instead of epoxidizing 6β-hydroxyhyoscyamine suggest that only a modest (~ 10°) shift in the Fe–O–H(C7) approach angle is sufficient to change the outcome. The observation that, in wild-type H6H, $^{2}H_2O$ solvent also increases the C7-hydroxylation:epoxidation ratio by ~ 8-fold implies that the latter outcome requires cleavage of the alcohol O-H bond, which, unlike in the LolO oxacyclization, is not accomplished in advance of C–H cleavage.

Introduction

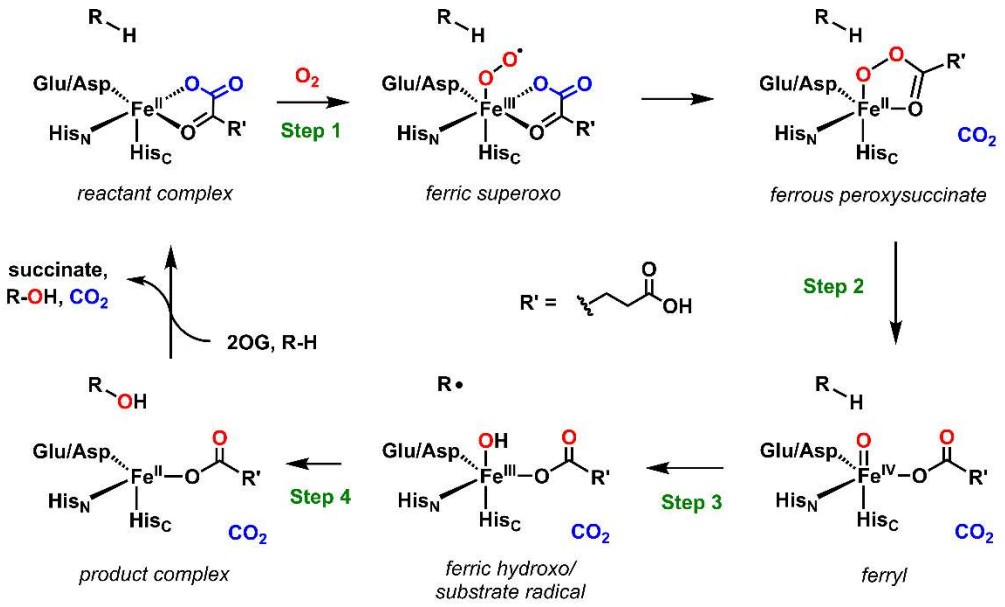

Scheme 1. Consensus mechanism for hydroxylation catalyzed by Fe/2OG dioxygenases.

The diversity and potential synthetic utility of reactions catalyzed by Fe(II)- and 2-oxoglutarate-dependent (Fe/2OG) oxygenases have made the enzyme superfamily an enticing platform for development of new biocatalysts.[1-2] The longest-known and most well-studied subclass of Fe/2OG enzymes, the hydroxylases (dioxygenases), can insert oxygen into strong C–H bonds (homolytic bond dissociation enthalpies of ~ 100 kcal/mol) with high regio- and stereo-selectivity.[3-4] Their conserved mechanism of action is largely understood (**Scheme 1**) and entails (1) activation of O_2 at the Fe(II) cofactor, leading to decarboxylation of 2OG and formation of a peroxysuccinatoiron(II) intermediate,[5-6] (2) peroxide heterolysis to form a succinate-coordinated oxoiron(IV) (ferryl) complex,[5,7-12] (3) abstraction of a hydrogen atom (H•) from the non-coordinating "prime" substrate (R-H) to form a state with a hydroxoiron(III) cofactor and adjacent substrate radical [Fe(III)–OH/R•],[8,12] and (4) coupling of R• with the iron-bound hydroxyl (known

as oxygen rebound)[13] to form the alcohol product and return the cofactor to its resting Fe(II) oxidation state.[4] In the reactions of Fe/2OG *mono*oxygenases from plants, fungi, and bacteria, different fates of the Fe(III)–OH/R• state (alternatives to step 4) lead to halogenation, desaturation, cyclization, ring-expansion and stereoinversion of aliphatic carbons.[14-18] With respect to biocatalysis and pharmaceutical synthesis, the abilities of certain Fe/2OG monooxygenases to install a halogen leaving group[14,19-20] for chemoselective fragment couplings or an epoxide electrophile[21-23] for covalent capture of biomolecular targets are among the most potentially valuable. The mechanism of the latter reaction type is less thoroughly understood than those of either hydroxylation or halogenation, providing motivation for this study.

The structure of the Fe/2OG halogenase SyrB2 from the syringomycin E biosynthetic pathway of *Pseudomonas syringae* showed that a crucial structural adaptation enabling halogenation is the absence of the carboxylate ligand of the His_2Asp/Glu "facial triad" of protein iron ligands[24] that had, prior to the discovery of the halogenases, been viewed as conserved across the enzyme superfamily.[25] The presence of a non-coordinating Ala or Gly at this sequence position opens a site for halide coordination to the Fe(II) reactant complex. The demonstration of an H•-abstracting *cis*-haloferryl intermediate in another halogenase, CytC3,[26] and then later in SyrB2[27-28] provided support for a halogenation mechanism analogous to that of hydroxylation but involving coupling of the R• to the halogen (Cl•/Br•) instead of the hydroxyl of the *cis*-Cl/Br–Fe(III)–OH complex. This mechanism raised the question of how the enzymes favor this alternative radical coupling over the oxygen-rebound step that was shown to be facile in related hydroxylases. The behavior of SyrB2 with altered substrates implied that an unusual disposition of the prime substrate's scissile C–H bond relative to the haloferryl complex results in very slow hydrogen-atom transfer (HAT) to the intermediate but then selective attack of the resulting R• on the cis-

coordinated halogen.[29] Substrate modifications perturbing this disposition unleashed more rapid HAT and competing hydroxylation.[29] Adjacent carbons of one particular substrate, the SyrB1 carrier protein bearing L-norvaline, exhibited different HAT rates and outcomes, with the less efficient H• donor (C4) retaining the capacity to be primarily halogenated and the more efficient donor (C5) undergoing solely hydroxylation.[29] A spectroscopic study then provided direct structural evidence for the correlation between substrate-cofactor disposition and both HAT efficiency and reaction outcome.[30] Several computational studies sought to delineate (1) the exact disposition that enables selective halogenation, (2) how the enzyme enforces this disposition by adjusting either the location of the substrate within the protein architecture, the coordination geometry of the haloferryl intermediate, or both, and (3) the nature of the frontier orbitals involved in the HAT and radical-coupling steps.[30-32] The conclusions of these studies have generally comported with the original hypothesis that control of substrate-intermediate disposition leverages the different spatial dependencies of competitive pathways for decay of the *cis*-halooxoiron(IV) intermediate (HAT from different donor sites) and its *cis*-halo-hydroxoiron(III) successor (different radical-coupling steps) to enable halogenation. Several of these studies proposed that formation of a haloferryl complex with "off-line" geometry[33-34] might be the key to establishing this special disposition.[32,35-37] In this geometry, the oxo group of the C–H-cleaving complex would occupy the site trans to the N-terminal histidine ligand (His_N) and be directed nearly perpendicular to the vector between the iron cofactor and prime substrate's scissile C–H bond, by contrast to its conventional "in-line" position trans to His_C and directed toward the C–H bond.

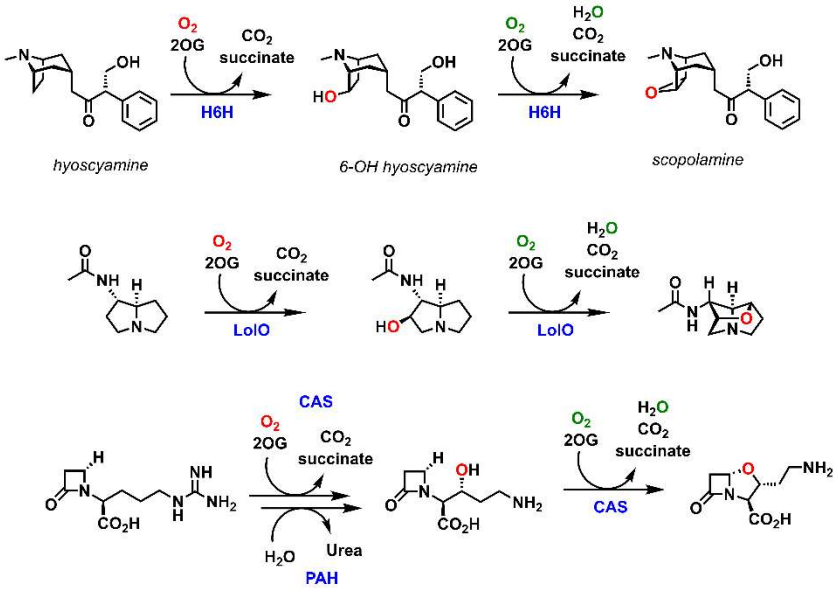

Scheme 2. Epoxidation and oxacyclization reactions catalyzed by H6H, LolO, CAS.

The two crucial control elements identified in halogenases – (1) an open coordination site on the iron cofactor suitably disposed to allow for coupling to the R• and (2) a special substrate-intermediate disposition that disfavors competing oxygen rebound – are potentially relevant also to oxacyclization reactions by Fe/2OG enzymes. Hyoscyamine 6β-hydroxylase (H6H), *N*-acetylnorloline synthase (LolO), and clavaminate synthase (CAS) all couple substrate oxygen atoms, which they install themselves in prior hydroxylation reactions, to neighboring carbons, thus forming epoxide, oxolane, and oxazolidine moieties, respectively.[16,23,38-41] In analogy to the Fe/2OG halogenases, coordination of the alcohol oxygen, leading to its deprotonation, could promote alkoxyl coupling to the carbon-centered radical of the substrate to form the oxacycle. Although the facial-triad carboxylate ligand is, by contrast to the case of the halogenases, conserved in these three enzymes, decarboxylation of 2OG during ferryl-intermediate formation vacates a site and could potentially allow for alkoxide coordination during the reaction.

Coordination might drive a change in the substrate-intermediate disposition (by changing the location of the oxo ligand of the ferryl complex, repositioning the substrate, or both) that could enable the ring-closure step to occur selectively. Appropriate positioning of the H•-donating carbon to make oxygen rebound slow would presumably still be required. As proposed for the halogenases,[30,32-33,35] formation of an off-line ferryl complex might potentially be an important factor in disfavoring rebound.

These hydroxylase/oxacyclase enzymes face the additional challenge of removing hydrogens from two different substrate carbons in sequential reactions. In principle, precise, static substrate positioning could ensure cleavage of the C–H bonds in the proper sequence. In this scenario, the substrate of the hydroxylation step would have both carbons poised for HAT to the first ferryl complex, but the site of hydroxylation (the first C–H bond to be cleaved) would be positioned more favorably, ensuring that it is preferentially targeted in the first step. After installation of the hydroxyl group at the first site, the less well-positioned second site could then donate H• to the second ferryl complex, albeit less rapidly. In this scenario, one might anticipate some off-pathway hydroxylation of the second site in the first step. Indeed, prior work with both H6H and LolO showed that out-of-order hydroxylation of the second site does occur.[42-43]

In this work, we used kinetic, structural, and spectroscopic approaches to interrogate both scopolamine-biosynthetic steps – 6β hydroxylation of hyoscyamine (Hyo) and 6,7-*exo*-epoxidation of 6β-hydroxyhyoscyamine (6-OH-Hyo) – catalyzed by H6H to determine how the enzyme switches both the C–H-cleavage site and the reaction outcome in its consecutive reactions. The results imply that H6H uses an elegantly simple strategy, in which the different intrinsic spatial dependencies of the competitive C–H-cleavage (C6 versus C7) and C–O-coupling

(rebound/hydroxylation versus epoxidation) steps are leveraged to enforce the two-step sequence in the absence of either major adjustment of substrate-cofactor disposition or substrate-alkoxide coordination in the second step. The results thus extend the principal conclusion of our studies on the halogenases – that substrate-cofactor disposition is of primary importance in the control of Fe/2OG-oxygenase regioselectivity and outcome – *even to this case of consecutive reactions targeting different carbons of the substrate for distinct outcomes*.

Results and Discussion

Equivalence of the rate-constants for HAT from C7 to the ferryl complexes in the hydroxylation and cyclization steps. We previously used stopped-flow absorption (SF-Abs) experiments to quantify pathways of ferryl-intermediate decay in the hydroxylation reaction catalyzed by the H6H homolog from *Hyoscyamus niger* (*Hn*H6H).[43] In that work, we explained that the observed rate constant for decay of the intermediate with each different substrate deuterium isotopolog (deuteriolog) studied corresponds to the sum of the elementary rate constants for all competitive decay pathways, and we resolved the rate constants for (H/D)AT from each carbon (C6 and C7, **Scheme S1**). In the present study, we carried out most of the experiments on the H6H homolog from *Atropa belladonna* (*Ab*H6H), because it afforded better yields in heterologous overexpression and purification (**Figures S1-S4**). Therefore, we first repeated the published kinetic analysis of the hydroxylation step using the *Ab*H6H and the suite of deuteriologs from the earlier work to assess whether we could justifiably consider data from the two closely related (90% identical, 95% similar) orthologs together. By SF-Abs measurements, we determined the elementary rate constants for HAT to the ferryl complex from C6 and C7 (k_{C6H} and k_{C7H}) to be 10 ± 0.1 s^{-1} and 0.5 ± 0.1 s^{-1} (5 °C), respectively (**Figure S5A, Table S1**), and, by LCMS analysis of

the products, we verified the consistency of these values with the ratio of C6:C7 hydroxylation (97:3; **Figure S5B, Table S2**). The similarity of both the individual rate constants and the product distributions for *Ab*H6H to those previously determined for *Hn*H6H (k_{C6H} = 14 s^{-1}, k_{C7H} = 0.5 s^{-1}; C6:C7 hydroxylation = 98:2) suggests that data from the two orthologs can be considered together.

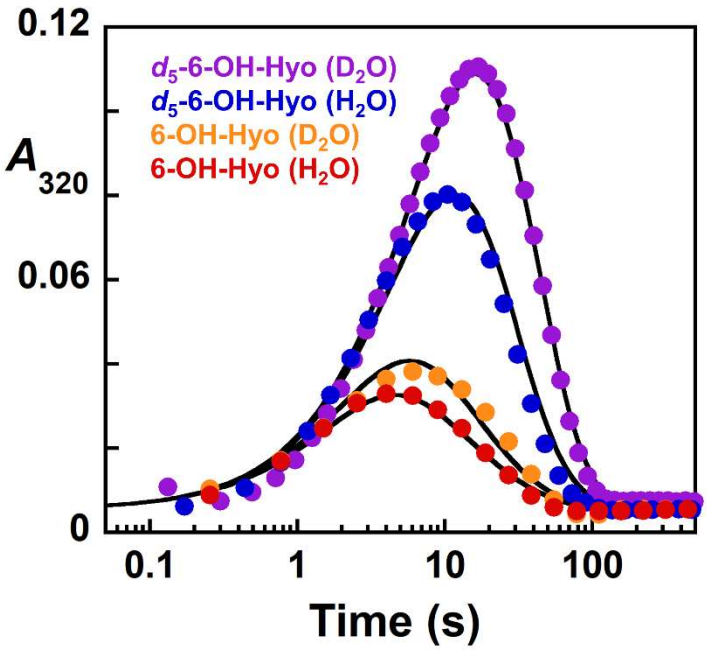

Figure 1. Impacts of substrate and/or solvent deuteration on the kinetics of formation and decay of the ferryl complex during the cyclization reaction catalyzed by *Ab*H6H. The four traces were globally simulated according to a two-step model with a second-order formation rate constant of 0.11 $mM^{-1}s^{-1}$ and four different observed decay rate constants: 0.49 ± 0.05 s^{-1} for 6-OH-Hyo in H_2O, 0.35 ± 0.04 s^{-1} for 6-OH-Hyo in D_2O, 0.11 ± 0.01 s^{-1} for d_5-6-OH-Hyo in H_2O, and 0.06 ± 0.01 s^{-1} for d_5-6-OH-Hyo in D_2O. The final concentrations after mixing were 0.55 mM *Ab*H6H, 0.5 mM Fe, 5 mM 2OG, 5 mM 6-OH or d_5-6-OH, and 0.19 mM O_2. A molar absorptivity of 1.7 $mM^{-1}cm^{-1}$ provided optimal agreement and is consistent with previous studies.[10,12,16,44-46]

We next undertook an analogous SF-Abs dissection of the cyclization reaction catalyzed by *Ab*H6H. When we rapidly mixed its reactant complex (*Ab*H6H•Fe^{II}•2OG•6-OH-Hyo) with a

buffer solution containing sub-stoichiometric O_2 (i.e., under single-turnover conditions), we observed the expected transient ultraviolet absorption with maximum change near 320 nm (**Figure S6)**, suggesting that the second reaction also accumulates a ferryl intermediate (a conclusion confirmed by freeze-quench Mössbauer experiments discussed below). Use of 6-OH-Hyo bearing deuteria on C7 (exo and endo) as well as C1, C5, and C6 (endo) (d_5-6-OH-Hyo, **Scheme S1**; see *Synthesis of Deuteriologs* in **Materials and Methods**) markedly increased the amplitude and slowed decay of the transient feature (**Figure S6**). We verified that this substrate D-KIE originates exclusively from the C7 deuteron by comparing kinetic traces obtained in reactions with 7-*exo*-d_1-6-OH-Hyo and d_5-6-OH-Hyo. That the resulting traces are effectively indistinguishable (**Figure S7**) justifies the use of either the less precious d_5-6-OH-Hyo or the more precious 7-*exo*-d_1-6-OH-Hyo interchangeably for kinetic experiments. The sluggishness of the oxacyclization reaction – especially with the 6-OH-Hyo deuteriologs – pushes the kinetic traces into a time regime (100-1000 s) that is plagued by a consistent physical artifact with our stopped-flow instrument. This artifact is more obvious in traces with small absorbance changes, such as those in **Figure S6** from reactions carried out under single-turnover reactions (i.e., with limiting O_2), than in traces with larger absorbance changes, such as those in **Figure S7** from reactions carried out with excess O_2. Although the crucial D-KIE is still clearly visible in the experimental absorbance-versus-time traces of the single-turnover reactions of **Figure S6**, the artifact interferes with more quantitative global analysis of the kinetic data. To enable such analysis, we subtracted polynomial backgrounds (**Figure S8**, *black solid lines*) from each trace, yielding the traces in **Figure 1**.

The rate constant for decay of the ferryl complex obtained by fitting and simulation of the corrected SF-Abs trace for the oxacyclization of protium-bearing 6-OH-Hyo is (0.5 ± 0.1 s^{-1}), ~ 20 times less than the 10 ± 0.1 s^{-1} seen for decay of the ferryl complex in the hydroxylation reaction,

which proceeds predominately by HAT from C6. It is, however, similar to the rate constant deduced for off-pathway abstraction of H• from C7 by the first ferryl complex, which leads to C7 hydroxylation. Use of 6-OH-Hyo substrate bearing deuterium slows decay of the ferryl complex to 0.1 ± 0.02 s^{-1}. This observed D-KIE of ~ 5 is sufficiently large to conclude that the ferryl complex cleaves the C7–H bond, but the *intrinsic* D-KIE on this step must be even larger, because uncoupling seen with the deuterated substrate implies that an unproductive and presumably hydrogen-isotope-insensitive step competes with HAT from C7 to contribute to decay of the ferryl complex. With the 7-d_1-6-OH-Hyo substrate, 2OG decarboxylation is only ~ 40% coupled to the scopolamine-yielding cyclization (assuming that the reaction with the protium-bearing 6-OH-Hyo is fully coupled) (**Figure S9**). The ~ 60% uncoupled ferryl decay has two implications. First, it means that the actual rate constant for productive deuterium transfer from the substrate is only ~ 0.04 s^{-1} (0.1 s^{-1} x 40%), yielding a D-KIE of > 10, which is more in line with values for HAT from carbon to ferryl complexes seen in prior studies.[10,15-16,28] Second, it implies that the observed rate constant of 0.5 ± 0.1 s^{-1} for ferryl decay with the protium-bearing substrate actually represents the sum of the elementary rate constants for uncoupled decay (~ 0.1 s^{-1}) and C7–H cleavage (0.4 s^{-1}). In other words, accounting for the uncoupling makes the rate constants for C7–H cleavage in the hydroxylation (0.3 ± 0.1 s^{-1})[43] and epoxidation (0.4 ± 0.1 s^{-1}) reactions even more similar. This similarity weighs against impactful differences in the positioning of the tropane core of the Hyo and 6-OH-Hyo prime substrates for the first and second reactions.

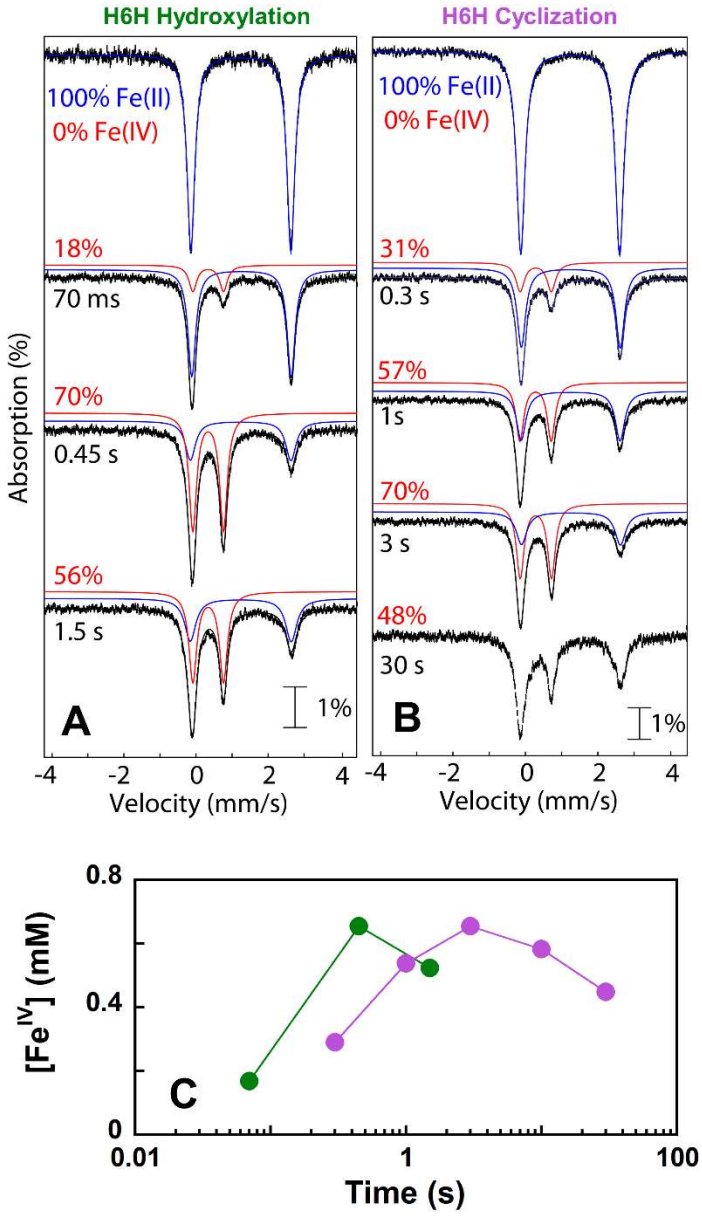

Figure 2. FQ-Mössbauer spectroscopic analysis of the two reactions catalyzed by *Ab*H6H. ***A-B***: Spectra (4.2-K/0 mT) of samples freeze-quenched at relevant reaction times in the hydroxylation (***A***) and oxacyclization (***B***) reactions. The final concentrations after mixing were 1.0 mM *Ab*H6H, 0.93 mM Fe(II), 4.0 mM 2OG, 24 μM Cld, 15 mM $NaClO_2$ and 2.0 mM of either 6-d_1-Hyo (***A***) or d_5-6-OH-Hyo (***B***). ***C***: Fe^{IV} concentrations determined by analysis of the Mössbauer spectra in panels ***A*** and ***B***. **Figure S10** shows that these kinetics approximately match the predicted kinetics

of accumulation and decay deduced from SF-Abs experiments under single-turnover conditions. Difficulty in determining the (supersaturating) O_2 concentration over time in experiments with the Cld/ClO_2^- O_2-generation system precludes a more precise assessment of the kinetic consistency of results from these multiple-turnover experiments with those from the single-turnover SF-Abs experiments.

Single ferryl complexes with standard Mössbauer parameters in the two sequential reactions. We used freeze-quench (FQ) Mössbauer spectroscopy to confirm the identities and compare the parameters of the UV-absorbing ferryl species in the two reactions of *Ab*H6H (**Figure 2** and **Table S3-S6**). As in previous studies of other Fe/2OG enzymes,[8,16,28,43] we used deuterium-bearing substrates to enhance accumulation of the intermediates. However, in the case of *Ab*H6H, formation of the ferryl complexes – particularly in the oxacyclization step – is so sluggish that a second intervention was required to enhance accumulation. In each well-studied case, formation of the ferryl complex in an Fe/2OG oxygenase has behaved as a second-order reaction, with no evidence of the accumulation of any preceding intermediate(s). This behavior implies that the first step, addition of O_2 to the cofactor, is rate limiting for ferryl-intermediate formation.[10,15-16,28,45] We verified the same behavior for the reactions of *Ab*H6H, showing that exposing either of its reactant complexes to super-saturating [O_2] (we estimate ~ 4 mM) by including catalytic (45 μM) chlorite dismutase (Cld, which converts ClO_2^- to O_2 and Cl^- very rapidly) in with the *Ab*H6H reactant complex and mixing this solution with excess $NaClO_2$ (15 mM)[47-48] increases both the rate of formation and the extent of accumulation of the ferryl intermediate (**Figure S10**). We used this procedure to initiate the *Ab*H6H reactions, and we rapidly froze samples at relevant reaction times for Mössbauer analysis.

The Mössbauer spectra of these freeze-quenched samples acquired at 4.2 K without an applied magnetic field (**Figure 2A**,**B**) reveal decay of the quadrupole-doublet signature of the

reactant complex (*top spectra*) and development of a new sharp quadrupole doublet – with parameters typical of ferryl complexes (*middle spectra*) – upon initiation of either reaction by the Cld/ClO_2^- O_2-generation system. The integrated areas of the decaying and developing features match and, at reactions times of 0.45 s for the hydroxylation reaction (**Figure 2A**) and 3 s for the cyclization reaction (**Figure 2B**), correspond to ~ 70% of the total ^{57}Fe absorption (**Figure 2C**). Increased reaction times gave loss of intensity of the narrow ferryl-associated doublets and re-development of Fe(II)-associated features (**Figure 2A**,**B**, *middle and bottom spectra*). In each reaction, the transient features could be adequately accounted for by a single quadrupole doublet with parameters typical of ferryl complexes detected in other Fe/2OG enzymes[9,15-16,27-28] (with the exception of the oxacyclization step of LolO discussed in the preceding paper[49]): δ = 0.32 mm/s and $|\Delta E_Q|$ = 0.85 mm/s for the hydroxylation reaction, and δ = 0.27 mm/s $|\Delta E_Q|$ = 0.86 mm/s for the oxacyclization reaction (**Figure S11**). An overlay of the appropriate experimental reference spectra from the two *Ab*H6H reactions illustrates the similarity of the Mössbauer spectra of the initiating ferryl complexes, which contrasts with the case of the ferryl intermediates observed in the sequential LolO reactions (**Figure S12**). In the case of LolO, we found HAT from C7 to the second ferryl intermediate state to be ~ 20-fold faster than HAT from C7 to the first ferryl complex, and we suggested that this acceleration results from the same change in coordination that engenders the unusual Mössbauer parameters (high values of δ and $|\Delta E_Q|$) in the dominant species of the second reaction's ferryl state. Analogously, the observation that the rate constants for C7–H cleavage by the ferryl complexes in the two *Ab*H6H reactions are indistinguishable (0.4 ± 0.1 and 0.3 ± 0.1 s^{-1}) suggests a common substrate-cofactor disposition, a conclusion that comports with the observation of ferryl intermediates with similar (and normal) parameters in the two reactions.

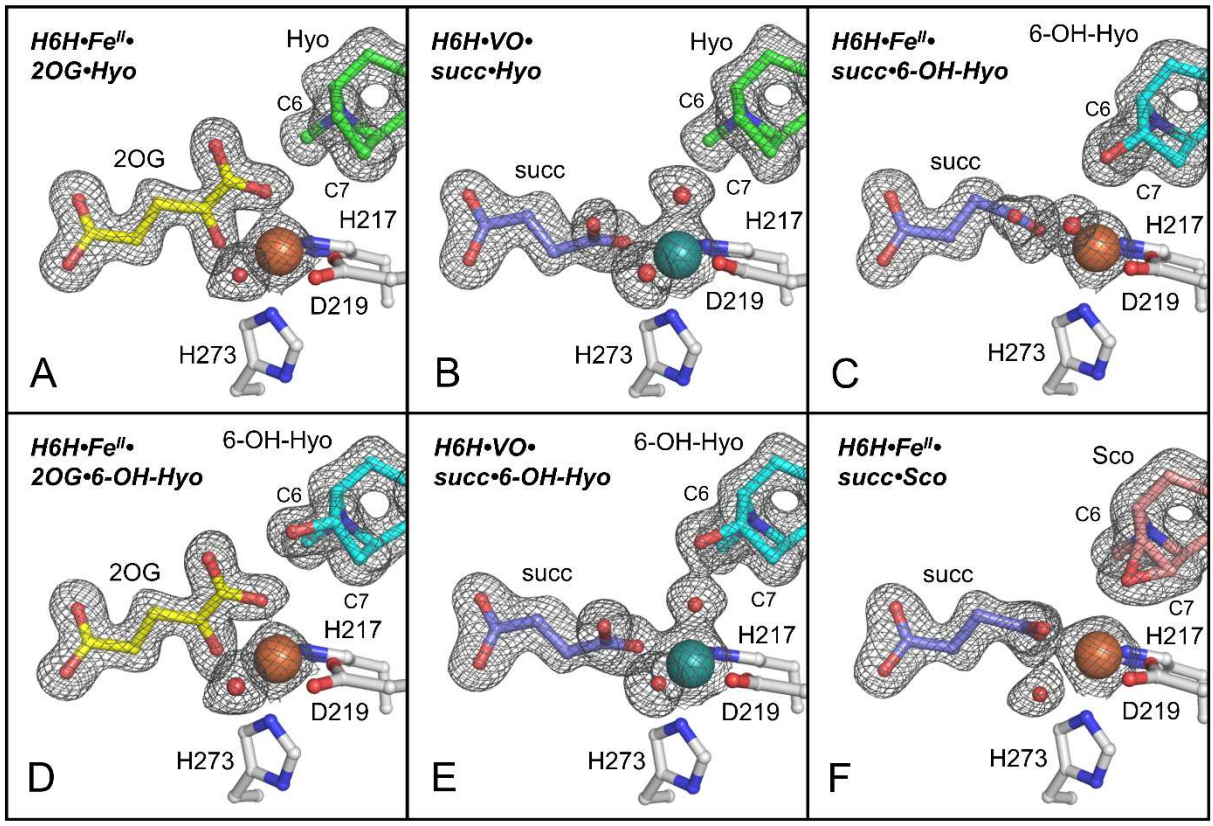

Figure 3. Active site of *Ab*H6H from crystal structures of (or mimicking) six different states in its hydroxylation-epoxidation reaction sequence. The six panels show zoomed views of the active-site facial triad, the metal cofactor (or mimic), the co-substrate/co-product, and the prime substrate/product from structures of the reactant (***A***, ***D***), vanadyl-derived (***B***, ***E***), and product (***C***, ***F***) complexes for the hydroxylation (***A***-***C***) and cyclization (***D***-***F***) reactions. In each panel, a $2F_o$-F_c electron density map contoured to 1.0 σ is shown as gray mesh. Selected side chains, water molecules, cofactors, substrates, co-substrates, and products are shown in ball-and-stick or sphere representation and colored according to atom type.

Multiple crystallographic views of the AbH6H active site implying invariant substrate positioning in its consecutive steps. We more directly assessed the possibility of different substrate positions in the two reactions by structural methods. X-ray crystallography afforded high-resolution global views of the relevant iron complexes, and complementary EPR-based

characterization of the H6H•vanadyl•succinate•(6-OH-)Hyo (succinate is hereafter abbreviated succ) complexes afforded both accurate active-site metrics relevant to reactivity and, importantly, a cross-check of the more global geometries seen in the crystal structures, *but with the metal in the +IV oxidation state*. A previously reported X-ray crystal structure of another H6H homolog from *Datura metel* (*Dm*H6H) in complex with 2OG and the hydroxylation substrate (Hyo) had Ni(II) in place of Fe(II), presumably to prevent turnover of the complex during crystallization and data collection.[50] To the best of our knowledge, neither the structure of the authentic O_2-reactive H6H•Fe^{II}•2OG•Hyo hydroxylation complex nor any structure with the oxacyclization substrate, 6-OH-Hyo, bound in the active site has been reported. We solved a series of six structures of wild-type (wt) *Ab*H6H in complex with either its iron cofactor or the vanadium mimic [oxovanadium(IV), prior to X-ray exposure] and appropriate combinations of substrates and products. The structures range in resolution from 1.53-1.79 Å, and they all show well-defined electron density for the metal ion, its ligands, and the substrates/products (**Figure 3**; statistics shown in **Tables S7** and **S8**). Overall, they reveal a nearly identical disposition of the prime substrate to the metal. The visualized atoms of the common tropane core of the Hyo and 6-OH-Hyo substrates occupy almost precisely the same positions in all six structures (**Figure S13**). The absence of more profound differences – especially in pairwise comparisons of analogous Hyo and 6-OH-Hyo complexes – is consistent with the kinetic and spectroscopic results discussed above.

The structures of the two reactant complexes [*Ab*H6H•Fe^{II}•2OG•Hyo and *Ab*H6H•Fe^{II}•2OG•6-OH-Hyo; **Figure 3A,D**] confirm the expectation that the prime substrates would share a common binding site; their tropane cores nearly superimpose. An interaction of the distinguishing C6 hydroxyl group of the oxacyclization substrate with 2OG is associated with a very minor (0.3 Å) shift of C6 relative to its position in the Hyo complex. As seen in the prior

structure of the *Dm*H6H•Ni^{II}•2OG•Hyo complex,[50] the 2OG carboxylate coordinates trans to H273, facing the C6 position of Hyo (**Figure 3A**,**D**). This binding mode is characterized as off-line,[33-34] because it leaves the presumptive O_2-addition site (occupied in the structures by a water ligand) roughly trans to H217 (His_N) and perpendicular to the Fe-C6 vector. Should the oxo group of the ferryl intermediate come to occupy this site (the simplest assumption), it would be poorly positioned to accept the C6 exo hydrogen. However, we view the available evidence on other Fe/2OG enzymes as implying that the position of the 2OG carboxylate in the reactant complex *does not* determine the position of the oxo ligand in the intermediate state: either a shift of the carboxylate in the process of O_2 addition[34,51] or second-sphere control of the trajectory of O–O-bond cleavage in the resulting peroxysuccinatoiron(II) intermediate[35] (which forms upon 2OG decarboxylation[5]) could net, in essence, replacement of the C1 carboxylate of 2OG by the ferryl oxo, yielding an in-line ferryl complex from off-line 2OG (or vice versa).

To assess the possibility that outcome-controlling structural differences between the hydroxylation and oxacyclization complexes might emerge during ferryl intermediate formation, we analyzed H6H complexes harboring the co-product (succ), the (6-OH-)Hyo prime substrate, and oxovanadium(IV) (vanadyl) in place of iron. Prior work on other Fe/2OG enzymes has shown that the stable vanadyl complexes structurally mimic the ferryl intermediates, both by adopting active-site configurations that correlate better with observed reaction outcomes than do the configurations of the reactant complexes and by reproducing substrate-association/dissociation dynamics of the ferryl complexes more closely than do the reactant complexes.[5,15,30,36,52-54] More recent computational work employing density function theory (DFT) to estimate relative coordination energies in small active-site models has raised caveats regarding the fidelity of ferryl mimicry by vanadyl,[36,55] but these studies have neither provided alternative explanations for the

experimental correlations of structure to reaction dynamics/outcomes nor accounted for the possibility that the larger protein structure could override small energetic differences in intrinsic propensity of the metal and ligands to adopt a certain coordination geometry.[15,52-53]

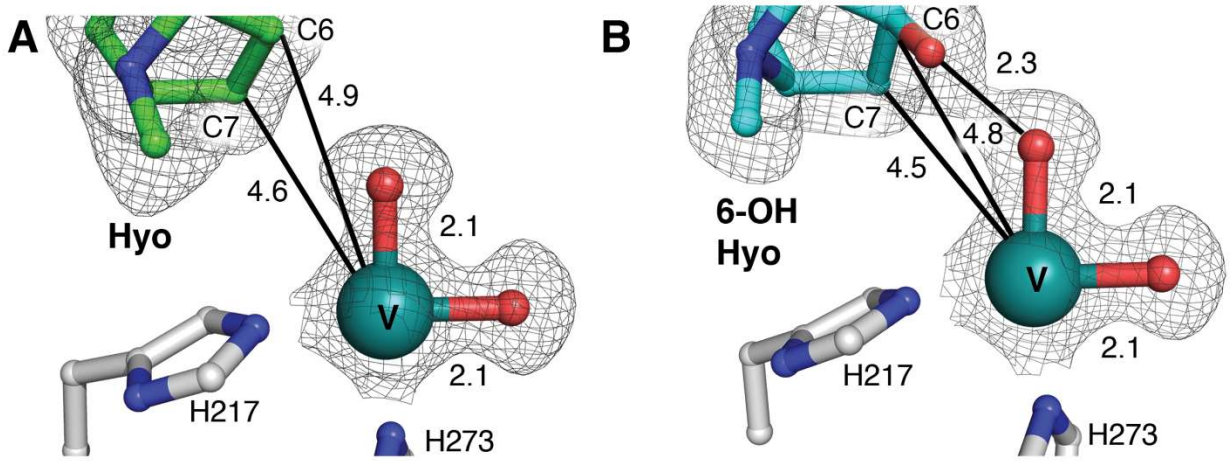

Figure 4. Comparison of the active sites in the vanadyl-derived complexes intended to mimic the ferryl intermediates of the hydroxylation (***A***) and epoxidation (***B***) reactions. The gray mesh illustrates $2F_o$-F_c electron density maps (contoured to 1.0 σ) for the vanadium and its two non-protein oxygen ligands. Selected side chains, water molecules, cofactors, substrates, co-substrates, and products are shown in ball-and-stick or sphere representation and colored according to atom type.

We solved structures from crystals of the *Ab*H6H•V^{IV}O•succ•Hyo and *Ab*H6H•V^{IV}O•succ•6-OH-Hyo complexes, the latter the first example of the use of the vanadium cofactor mimic to provide structural insight in a native non-hydroxylation reaction.[5,53,56] Our structural models indicate that, as in the prior studies, the otherwise stable vanadyl ion undergoes photoreduction to V(III) or V(II) during data collection (**Figure 4A** and **B**).[5,53] Specifically, the shortest V-O distance of 2.1 Å is longer than the expected 1.6-Å V^{IV}≡O bond of

vanadyl,[52]implying a lower metal oxidation state.[52] Surprisingly, there are *two* distinct lobes of electron density attributable to non-protein (presumably, oxygen) ligands. One of the lobes occupies the in-line-oxo position (trans to H273) and projects toward the substrate. The second is cis to the first, in the off-line position (trans to H217). We considered two alternative explanations for the presence of two H_xO ligands. First, it could reflect ambiguous binding of the vanadyl ion in two different orientations in the crystal.[55] However, in refinements to address this possibility, both ligands refined to full occupancy (meaning that both sites are fully occupied at the same time) in both structures, weighing against this explanation. Second, it is possible that a solvent ligand coordinates cis to the vanadyl oxo and becomes chemically equivalent to the oxo as a consequence of photolytic V^{IV} reduction during data collection. Although such metal hydration associated with photoreduction has not been observed in other crystal structures of Fe/2OG enzymes derived from vanadyl complexes, we considered that the unusual solvent channel adjacent to the metal ion in the H6H active site could enable it here (see **Figure S14**).[5,43,53,56] In this scenario, it would be important to know which oxygen in the structure corresponds to the oxo and which corresponds to the water in the original vanadyl complex, especially given the hypothesis advanced in other studies that formation of an off-line ferryl complex can be important to controlling the reaction outcome.[30,35,57] Fortunately, in addition to its ability to mimic traits of the ferryl states in these enzymes, the $S = 1/2$ vanadyl ion is also useful as an EPR spin probe for experiments that can, in favorable cases, define the orientation of the metal-oxo axis in the actual ferryl mimicking state.[5,52] Given the importance of this question to mechanistic interpretation, we present the results of such experiments before returning to further analysis of the structures.

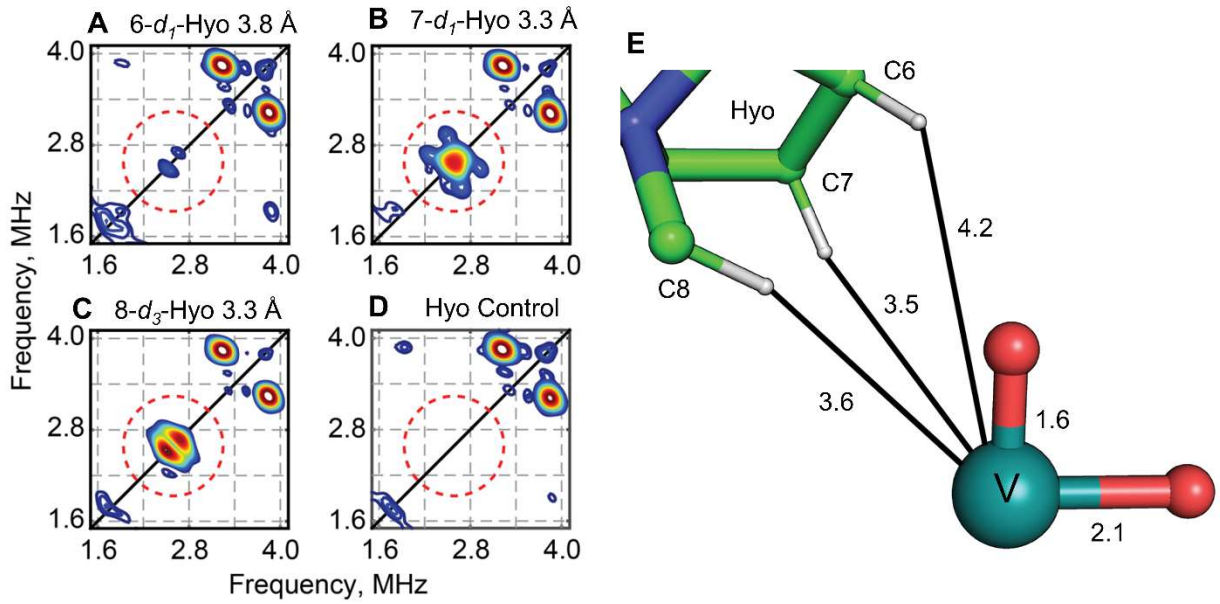

Figure 5. ^{2}H-HYSCORE spectra of *Hn*H6H•VO•succ•d_x-Hyo complexes containing 6-d_1-Hyo (***A***), 7-d_1-Hyo (***B***), 8-d_3-Hyo (***C***), or unlabeled hyoscyamine (***D***). The red-dashed lines encircle the expected positions of signals arising from deuterium nuclei. Spectra were collected at 396 mT and 35 K with microwave frequency 9.434 GHz. (***E***) V–O-contracted *Ab*H6H•V^{IV}O•succ•Hyo crystallographic model, with the three measured distances shown for comparison to the values determined from the HYSCORE spectra. The vanadium, oxygen ligands, and substrate are shown in ball-and-stick or sphere representation and are colored according to atom type.

Table 1. Distances and angles measured by ^{2}H-HYSCORE spectroscopy and cognate measurements derived from X-ray crystal structures for comparison.

	^{2}H-HYSCORE	**Crystal Structures**
Hyo		
V–^{2}H(C6) (Å)	3.8 ± 0.3	4.2 ± 0.2
V–^{2}H(C7) (Å)	3.3 ± 0.1	3.5 ± 0.2
V–^{2}H(*N*-Me) (Å)	3.3 ± 0.1	3.6 ± 0.2
O–V–^{2}H(C7) (°)	40 ± 5	49.2 ± 5[a]
V-O/C7-^{2}H Angle (°)	25 ± 2	26.1 ± 0.2
6-OH-Hyo		

V–^{2}H(C7) (Å)	3.4 ± 0.1	3.5 ± 0.1
O–V–^{2}H(C7) (°)	40 ± 5	51.8[a]
V-O/C7-^{2}H Angle (°)	25 ± 2	25.4 ± 0.2

[a]After contraction of the in-line V-O bond to 1.6 Å

Hyperfine sublevel correlation (HYSCORE) spectra reveal in-line vanadyl in the complex with either prime substrate. We used HYSCORE spectroscopy to interrogate the dipolar interaction between the S = 1/2 vanadyl ion and deuterium (^{2}H) nuclei placed at different locations in the prime substrates of H6H. For the hydroxylation complex (with Hyo), we used three different substrate deuteriologs – 6-d_1-, 7-d_1-, and 8-d_3-Hyo (C8 is the *N*-methyl). As described previously,[5,15,30] the splitting in the HYSCORE spectra can be related to the V–^{2}H distance. Analysis of the spectra of the *Hn*H6H•V^{IV}O•succ•Hyo complexes yielded distances of 3.8 ± 0.3, 3.3 ± 0.1, and 3.3 ± 0.1 Å from the metal to the deuteria on C6, C7, and C8, respectively (**Figure 5** shows representative data; **Figures S15-S21** show the full set of field-dependent ^{2}H-HYSCORE spectra with simulations). To compare these distances to those predicted from the X-ray crystal structure, we added hydrogens to C6-8 of Hyo at standard C–H distance and angles (**Figure 5**, *right*). The ^{2}H-HYSCORE metrics agree well with the corresponding distances of 4.2 ± 0.2, 3.5 ± 0.2, and 3.6 ± 0.2 Å in the hydrogens-added model (**Table 1**). The fact that the C7 and C8 hydrogens are slightly closer to the metal than the C6 exo hydrogen that is the primary H• donor to the ferryl complex emphasizes the importance of approach angle to HAT efficiency. This notion was first put forth in our work on the halogenase SyrB2,[29] has been supported by multiple computational studies reported since,[32,55,58] and is discussed in more detail below.

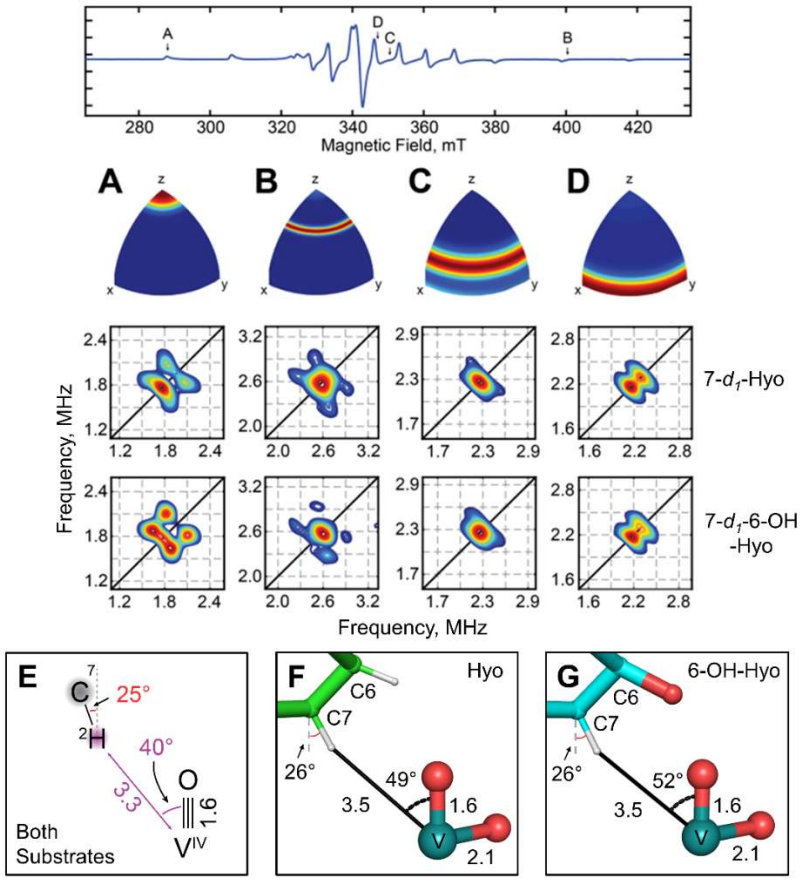

Figure 6. Comparison of ^{2}H-HYSCORE patterns observed for the vanadyl complex of *Hn*H6H with either 7-d_1-Hyo (*upper spectra*) or 7-d_1-6-OH-Hyo (*lower spectra*) at (***A***) 280 mT, (***B***) 396 mT, (***C***) 344 mT, and (***D***) 340 mT. Orientation selectivities probed by each magnetic field position (*blue plots at top of* ***A*****-*****D***) are color coded (red - fully excited; blue, not excited). Magnetic field positions at which the spectra were acquired are indicated by black arrows on the one-dimensional EPR spectrum (*very top*). Panel ***E*** shows the metrics extracted from simulation of the ^{2}H-HYSCORE data, all identical for both substrates, including the O–V–^{2}H(C7) angle (40°), the V–^{2}H separation (3.3 Å) and the angle between the C7–^{2}H bond and the V–O vector (25°). Panels ***F*** and ***G*** show the V–O-contracted *Ab*H6H•VO•succ•(6-OH-)Hyo crystallographic models, with measurements displayed to enable comparison to the values obtained by the ^{2}H-HYSCORE analysis. The vanadium, oxygen ligands, and substrate are shown in ball-and-stick or sphere representation and colored according to atom type.

For the *Hn*H6H•V^{IV}O•succ•7-d_1-Hyo complex, the angle relating the *g*-tensor of the vanadyl spin probe and the metal-deuterium vector was also accessible by analysis of the magnetic field-dependence of the spectra (**Figure S15-S21**). The *g*-tensor of vanadyl aligns with the V≡O bond, allowing the spin-frame angle to be straightforwardly related to the molecular frame (**Figure 6**). The O–V–^{2}H(C7) angle obtained through this analysis is 40 ± 5° (**Figure 6**, **A-D**, *middle*). In the hydrogens-added *Ab*H6H crystallographic model, the O–V–^{2}H(C7) angle is ~ 50° for the in-line oxygen ligand but ~ 130° for the off-line oxygen ligand (**Figure 6F** and **S22**). Only the former value is consistent with the HYSCORE spectra (**Figure 6**, **E-G** and **Table 1**).[26,28,59-60] In the event that the off-line oxygen ligand were actually the vanadyl oxo, this ~ 130° angle would have resulted in patterns (**Figure S23**) very different from those observed in **Figure 6**. The HYSCORE data thus establish that, of the two non-protein oxygen ligands seen in the structure of the *Ab*H6H•V•succ•Hyo complex, the in-line oxygen is derived from the vanadyl oxo group, implicating (as expected) an in-line ferryl complex in the hydroxylation reaction.

The equivalent field-dependent HYSCORE spectra for the *Hn*H6H•V^{IV}O•succ•7-d_1-6-OH-Hyo (oxacyclization) complex are *essentially identical* to those for the *Hn*H6H•V^{IV}O•succ•7-d_1-Hyo (hydroxylation) complex (**Figure 6**, **A-D**, *compare bottom to middle*). These data further validate the observation from the crystal structures that the hydroxylation and cyclization substrates are positioned almost identically, and they are also irreconcilable with an off-line vanadyl, which would lead to very different spectra (**Figure S24**). Indeed, the HYSCORE data impose relatively tight restraints on the possible positions of the vanadyl oxo in both complexes (**Figure S25,** *red mesh*).

The detailed HYSCORE analysis of 7-d_1-(6-OH-)Hyo-containing complexes also afforded a relatively accurate extraction of ^{2}H nuclear quadrupole-coupling parameters, yielding the angle between the C7–^{2}H and V–O vectors (25 ± 5°) in both complexes. This estimate agrees well with that from the crystal structures (26° in both complexes; **Figure 6**). The relatively weak signals for the C6 deuteron precluded a meaningful estimate of either the O–V–^{2}H(C6) angle or the C6–^{2}H/V–O vector angle for either complex, but the data are consistent with the small angles seen in the crystallographic models (10-20°). The ^{2}H-HYSCORE results are thus fully consistent with the crystallographic models and, most importantly, with a single, in-line binding mode for the vanadyl ion.

Target-hydrogen approach angle correlates with HAT efficiency in H6H and related enzymes. As noted, the structures solved from crystals of the *Ab*H6H•V^{IV}O•2OG•(6-OH-)Hyo complexes reveal the V(IV) photoreduction seen in prior work.[5,53,56] Even under the assumption that vanadyl is a faithful mimic of the catalytically relevant ferryl state (as the biochemical data suggest[15,52-53]), the elongated V–O bond seen in the structures would necessarily distort the measured (V)O–H(C6/7) distances and O–V–H(C6/7) angles. These metrics are (again, under the assumption of accurate mimicry) most relevant to HAT kinetics/regioselectivity and for considering possible epoxidation mechanisms.

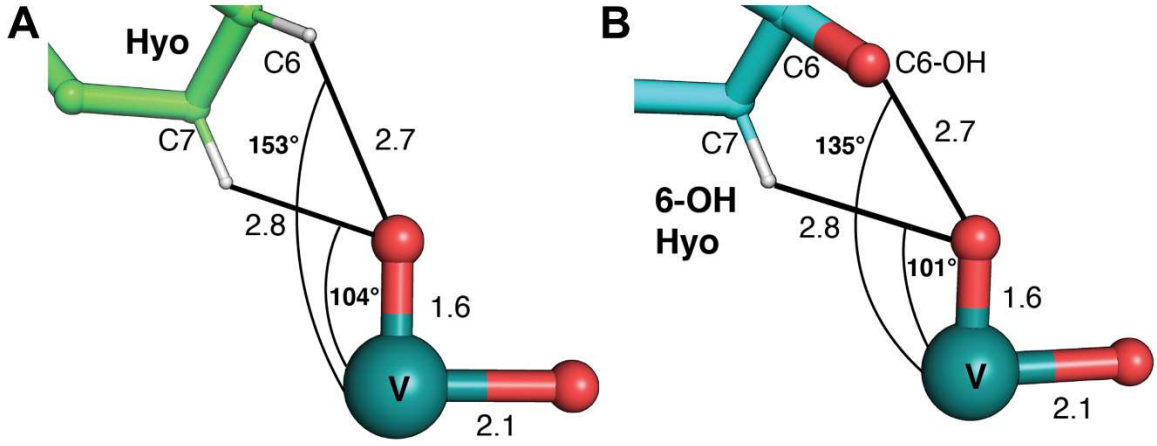

Figure 7. Comparison of key metrics in the structural models of the (***A***) *Ab*H6H•V^{IV}O•succ•Hyo and (***B***) *Ab*H6H•V^{IV}O•succ•6-OH-Hyo complexes obtained by adding hydrogens to the experimentally observed prime substrates and shortening the observed V-O distances to 1.6 Å. Selected side chains, water molecules, cofactors, substrates, co-substrates, and products are shown in ball-and-stick or sphere representation and colored according to atom type.

Table 2. Metrics from vanadyl-complex-derived crystal structures of Fe/2OG enzymes along with measured HAT rate constants and fractions of ^{18}O incorporation from $^{18}O_2$ into hydroxylated products.

	Enzyme[a]	**TauD**	**VioC** *+ L-Arg*	**CAS** *+ DGPC*[b]	***Ab*H6H (C6)** *Hyo*	***Ab*H6H (C7)** *Hyo*	***Ab*H6H (C7)** *6-OH-Hyo*	***L289F Ab*H6H (C7)** *6-OH-Hyo*
Unaltered (V-O > 1.6 Å)	**V-O Distance (Å)**	1.9[d]	1.9[e]	1.9[f]	2.1[g]	2.1[g]	2.1[g]	1.7[g]
	V-O-C Angle (°)	136	132	134	139	113	108	127
	(V)O-H(C) Distance (Å)	1.8	2.4	2.1	2.3	2.6	2.7	2.8

Altered (V-O = 1.6 Å)	**V-O-H Angle (°)**	125	129	137	151	97	91	111
	(V)O-H(C) Distance (Å)	2.0	2.5	2.3	2.7	2.8	2.7	2.8
	V-O-H Angle (°)	132	134	142	153	104	101	112
	V-O/C-H Angle (°)	28	57	53	78	26	26	16
	k_{HAT} (s^{-1})[c]	15[h]	10[i]	18	10	0.3	0.4	N.D.
	^{18}O from $^{18}O_2$ (%)	N.D.	98[i]	96	87[j]	34[j]	13	42
	PDB	6EDH	6ALR	6VWR	8CV9	8CV9	8CVC	8CVH

[a]Fe/2OG enzymes structurally characterized in their V•succ•substrate complexes for which either % ^{18}O or k_{HAT} reported here or previously; [b]Hydroxylated at C3; [c]5°C; [d]Reference 53; [e]Reference 15; [f]Reference 56; [g]This work; [h]Reference 8; [i]Reference 44; [j]Reference 43.

To better correlate the observed chemistry and HYSCORE data with the crystal structures, we further analyzed the structures under the assumption that V(IV) photoreduction at 100 K in the crystal causes only V–O bond elongation. This approximation has support from a prior study.[5] We thus manually shortened the bond back to 1.6 Å, the M–O-bond length determined for both vanadyl and ferryl intermediates,[26,28,59-60] by moving the oxygen toward the metal (**Figure 7A, B**). Interestingly, although HAT from C6 of Hyo to the hydroxylation ferryl complex is considerably faster (10 s^{-1}) than HAT from C7 (0.3 s^{-1}), the C6 and C7 exo hydrogens are nearly equidistant from the oxo ligand in the resultant vanadyl/ferryl model (2.7 Å versus 2.8 Å, respectively). The ~ 30-fold difference in their rate constants can be explained by their different approach angles. The approach angle for the C6 exo hydrogen [V–O–H(C6); note that this angle is different from, but straightforwardly related to, the O–V–^{2}H angle afforded by HYSCORE and shown in **Figure 8**] is 153°, which is considerably larger than the approach angle of the C7 exo hydrogen [V–O–

H(C7) = 104°]. The larger angle for the preferred hydrogen is consistent with computational studies suggesting that the angle between the Fe^{IV}=O bond and the substrate hydrogen controls the FMOs engaged (σ- versus π-pathway) and thus the HAT barrier height, with σ-pathway-enabling obtuse angles giving more efficient HAT.[32,55,58] More recent analysis has suggested that, even within the σ manifold, the more acute angles lead to slower HAT.[37]

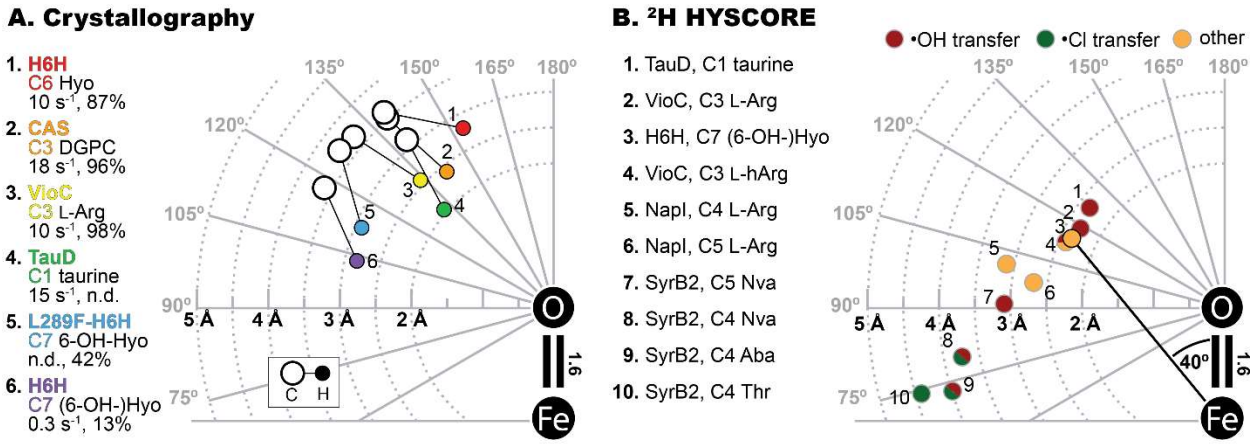

Figure 8. Depiction of the disposition of targeted C–H bonds relative to the metal-oxo cofactor from either (***A***) vanadyl-derived, V–O-bond contracted crystallographic models of enzymes with known HAT rate constants or ^{18}O incorporation[5,44,46,53,56] or (***B***) ^{2}H-HYSCORE spectroscopy.[5,15,30,53] Panel ***A*** shows the seven reactions shown in **Table 2**. The approach angle of H to the vanadyl/ferryl unit correlates with both the HAT rate and % ^{18}O incorporation, while the O-H distance and the angle between the C–H and metal-oxygen (M–O) vectors do not. The O-H and O-C distances, V-O-H angles, and V–O vector/C–H vector angles are drawn to scale; the ferryl bond length is 1.6 Å and each C–H bond is 1.09 Å. Carbon atoms are depicted as squares and hydrogen atoms as circles. Panel B shows the distance and angle determined by ^{2}H-HYSCORE spectroscopy utilizing either an $[Fe\text{-}NO]^{7}$ complex (SyrB2[30]) or the vanadyl ion (all others[5,15,53]) as a spin probe. ^{2}H-HYSCORE directly measures the O-M-^{2}H angle and the M-^{2}H distance; these two metrics along with the metal-oxygen bond length of 1.6 Å forms a triangle that readily allows the M-O-^{2}H angle to be determined, and these angles are depicted in the figure to simplify visual comparison to the metrics derived from crystallography. The experimentally determined O–M–H angle and the calculated M–O–H angle for C7 of H6H are both indicated as an example.

To test this idea further, we compared our vanadyl-derived ferryl models of H6H to those that we could generate from reported structures[5,53] (and one other that we solved here[56]) of other Fe/2OG enzymes. The analogously formulated vanadyl-derived models of the hydroxylating ferryl complexes in TauD,[53] VioC,[5] and CAS[56] (in complex with deoxyguanidinoproclavaminate) all exhibit V–O–H angles (132-142°) and (V)O–H distances (2.0-2.5 Å) more similar to those for the C6 exo hydrogen than to those for the C7 exo hydrogen in the *Ab*H6H hydroxylation complex (**Table 2**, **Figure 8A** and **S26**). Accordingly, the hydroxylation reactions of TauD,[10] VioC,[44] and CAS (**Figure S27**) are all associated with relatively fast HAT steps, in addition to high incorporation of ^{18}O from $^{18}O_2$ into the prime product (**Figure 8A** and **Table 2**), which we previously showed to be a hallmark of efficiency in the HAT and oxygen-rebound steps.[43] In the vanadyl-derived model of the *Ab*H6H oxacyclization complex (with 6-OH-Hyo), the disposition of the C7 exo hydrogen remains nearly identical [O–H(C7) = 2.8 Å, V–O–H(C7) = 101°] to that in the hydroxylation model (with Hyo), comporting with the similarity of the measured rate constants for C7–H cleavage in the two reactions.

The *Ab*H6H•V•succ•6-OH-Hyo structure also reveals that the C6-oxygen does not directly ligate the metal, consistent with the lack of unusual Mössbauer parameters for the ferryl analog of this complex and further weighing against a previously proposed mechanism for oxacyclization, in which coordination by the C6 oxygen facilitates the C7-O coupling step. Instead, the C6 oxygen appears to form a very short (2.3 Å) hydrogen bond with the in-line oxygen ligand (**Figure 4B**). Although structures of vanadyl-derived complexes of other Fe/2OG enzymes have exhibited H-bonding between the substrate and the corresponding oxygen ligand, their extreme proximity in the *Ab*H6H complex with the cyclization substrate is unusual and potentially mechanistically relevant. In the V–O-contracted model for the *Ab*H6H oxacyclization complex, the separation

between the C6-OH and in-line O ligand becomes 2.7 Å, more typical of a normal hydrogen bond (**Figure 7B**). The 2.3-Å separation observed in the experimental structure might simply be an artifact of the V–O elongation that occurs upon photoreduction, but the closer proximity caused by the decrease in metal oxidation state could also mirror events in the actual oxacyclization reaction mediated by the second ferryl complex. Upon cleavage of the C7–H bond, the oxidation state of the iron would – in the mechanism adhering most closely to precedents – change from Fe(IV) to Fe(III), thus elongating the metal-oxygen bond similarly to V(IV) photoreduction. This step would move the hydroxo ligand toward the C6 hydroxyl group, possibly enabling proton transfer or formation of a low-barrier H-bond between the alcohol and the ligand prior to, or concomitantly with, C7–O(C6) bond formation. The observed substrate-cofactor disposition could thus be critical to achieving epoxidation and suppressing C7 hydroxylation (by oxygen rebound) in the second step.

As one additional corroboration that the active-site configurations seen in the crystal structures of the reactant and ferryl-mimicking vanadium complexes with 6-OH-Hyo accurately reflect the configurations that yield the epoxidation outcome, we also solved the structure of the *Ab*H6H•Fe^{II}•succ•Sco product complex (**Figure 3F**). The fact that the tropane core of the epoxide product closely overlays with that of the 6-OH-Hyo substrate in the reactant and intermediate-mimicking complexes (**Figure S13C**) again implies that substrate repositioning within the active site is not integral to the enzyme's promotion of epoxide-ring formation.

Overall, a consistent view of the two reactions catalyzed by H6H emerges from the results of these four distinct lines of inquiry, encompassing resolution of the C7–H cleavage rate constants in each reaction by SF-Abs and LCMS analysis, direct observation of the single ferryl intermediate formed in each reaction by FQ-Mössbauer experiments, and structural characterization of vanadyl

models for the ferryl complexes by X-ray crystallography and ^{2}H-HYSCORE spectroscopy. We conclude that H6H binds its pair of substrates in a single, conserved disposition to the cofactor that is more favorable for C6–H cleavage but allows for C7–H cleavage in the second step, after C6 has been "blocked" by hydroxylation in the first step. The obvious implication is that the observed disposition is almost certainly special – and possibly *unique* – in enabling the sequential H6H reactions resulting in epoxide installation. This hypothesis comports with the emerging evidence from prior structural analyses that substrate-cofactor disposition is generally crucial to reaction outcome in Fe/2OG oxygenases (**Figure 8B**).[55]

Sterically Perturbing L289F Substitution Disables Epoxidation, Unleashes Second Hydroxylation. In light of the nearly invariant substrate positioning, we posited that modestly sterically perturbing amino acid substitutions in the active site could derail the reaction sequence without abolishing the enzyme's activity outright. By screening variants with substitutions close to the prime substrate (as described in the *Supporting Information*), we identified the L289F variant (**Figure S28**) as exhibiting the predicted behavior and compared its catalytic capabilities with those of the wt *Ab*H6H enzyme. To set the baseline for comparison, we showed that wt *Ab*H6H could almost fully consume one equivalent of Hyo upon incubation with ≥ 1.5 equiv 2OG in an assay open to the air (**Figure S29**, *top right, blue and red bars*). The small residual peak at the elution time and *m*/*z* value of the Hyo substrate was not further diminished by increasing 2OG:Hyo ratios (up to 3 equiv), suggesting that it reflects the presence of a contaminant with a similar structure and identical mass (e.g., the enantiomer of Hyo). At high 2OG:Hyo ratios, substrate consumption was accompanied by the development of a dominant new LCMS peak with a change in mass-to-charge ratio, Δ*m/z*, of +14 relative to Hyo (**Figure S29**, *top right, green bars*). The co-elution of the

associated species with authentic scopolamine confirmed that this dominant product forms by the hydroxylation-epoxidation sequence, which can be completed in the presence of sufficient 2OG (**Figure S29**; *top left*). The primary product that developed at lower 2OG:Hyo ratio had Δ*m*/z = +16 and co-eluted with 6-OH-Hyo (*red bars*). Its yield exhibited the expected initial rise with increasing 2OG:Hyo ratio up to a value of ~ 1.2, at which point its subsequent conversion to Sco resulted in a decrease in yield with increasing 2OG:Hyo. We also detected three minor products (**Figure S29**, *middle panels*), which we identified by their Δ*m*/*z* values and co-elution with standards as 7-OH-Hyo (Δ*m*/*z* = +16), 6,7-dehydro-Hyo (Δ*m*/*z* = -2), and 6,7-$(OH)_2$-Hyo (Δ*m*/*z* = +32). Because the small quantity of 7-OH-Hyo that is formed by out-of-order C7 targeting in the first reaction is not processed further (**Figure S29**, *yellow bars*), the 6,7-$(OH)_2$-Hyo product must reflect C7 hydroxylation in competition with 6,7-epoxidation in the second reaction. Indeed, the dihydroxylated product was also readily detected in *Ab*H6H reactions with 6-OH-Hyo (**Figure S29**, *bottom left panel*). In either the two-step conversion starting from Hyo or the direct conversion of 6-OH-Hyo, the epoxide product was found to predominate by a factor of ~ 25 over the 6,7-dihydroxylation product.

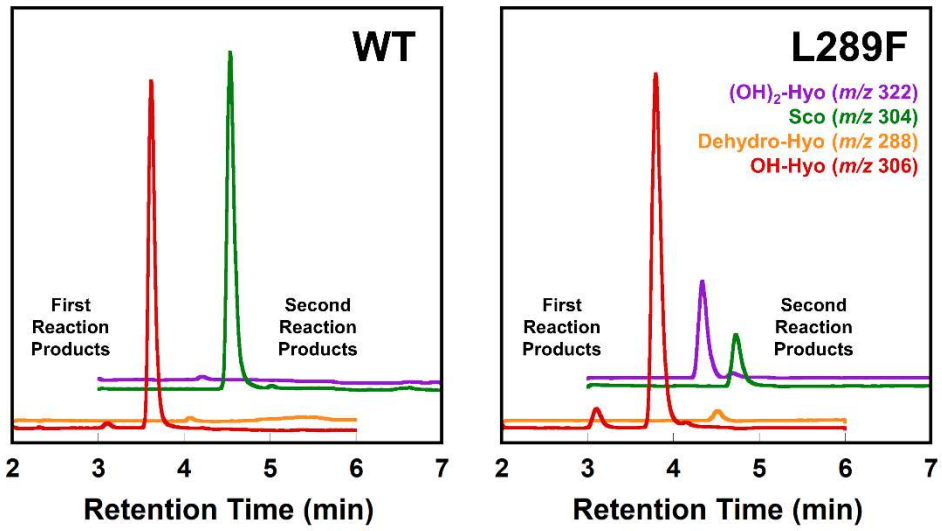

Figure 9. LCMS analysis of products in reactions of wt and L289F *Ab*H6H with either Hyo or 6-OH-Hyo. The red trace shows *m/z* = 306, corresponding to two products, 7-OH-Hyo, with retention time of 3.1 mins, and 6-OH-Hyo, with retention time of 3.8 mins. The orange trace shows *m/z* = 288, corresponding to the 6,7-dehydro-Hyo minor product. The green and purple traces depict *m/z* = 304 and *m/z* = 322, respectively, corresponding to the Sco and $(OH)_2$-Hyo products. The final concentrations were 0.12 mM enzyme, 0.1 mM Fe, 0.1 mM prime substrate, and 0.03 mM 2OG. Assays were allowed to proceed for 1 h at 4° C open to the air.

Analogous assays of the *Ab*H6H L289F variant revealed that it retains 6β-hydroxylase activity toward Hyo and exhibits regioselectivity for C6 over C7 similar to that of wt *Ab*H6H. LCMS analysis gave a product distribution of 95 ± 1.2% 6-OH-Hyo, 3 ± 0.7% 7-OH-Hyo and 2 ± 0.9% 6,7-dehydro-Hyo following reactions of the variant with 1 equiv Hyo and 0.3 equiv 2OG at 4 °C for 1 h under air. By contrast to its wt-like behavior toward Hyo, we found the L289F variant enzyme to be drastically compromised in epoxidation of 6-OH-Hyo and instead to promote primarily 7-hydroxylation in its second reaction, yielding 3:1 6,7-$(OH)_2$-Hyo:Sco. Given that wt *Ab*H6H forms the two products in a ~ 1:20 ratio, the L289F substitution enhances 7-hydroxylation of 6-OH-Hyo by a factor of ~ 60 in its competition with 6,7-epoxidation (**Figure 9**). The

observation of the dihydroxylation product weighs heavily against previous proposals that oxygen rebound to C7 in the second reaction is disfavored for steric or stereoelectronic reasons relating primarily to the structure of the 6-OH-Hyo epoxidation substrate itself rather than by its interaction with the enzyme.[61] Clearly, the enzyme actively impedes reaction flux away from an inherently feasible second hydroxylation pathway to direct the strain-incorporating epoxidation outcome.

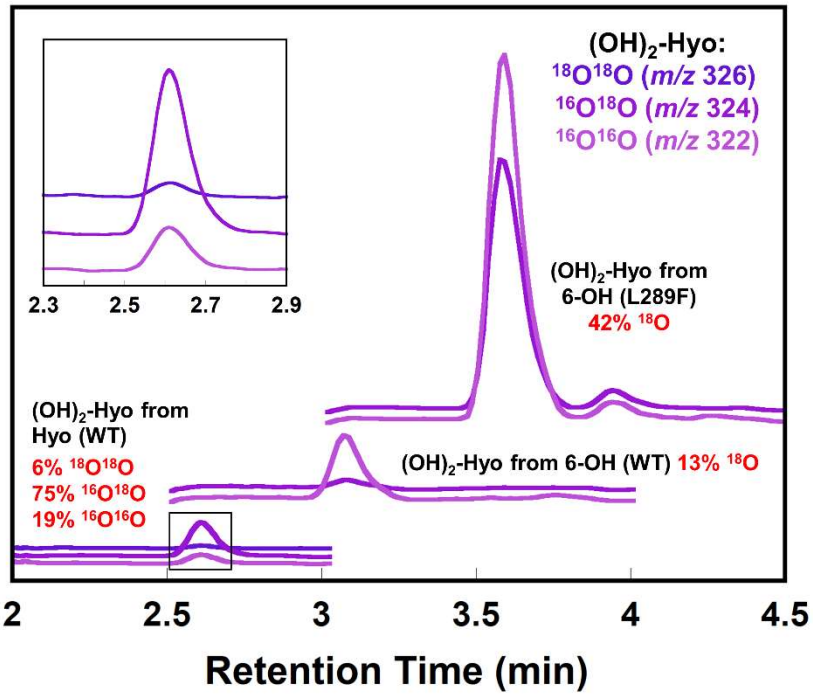

Figure 10. LCMS chromatograms showing the composition of the dihydroxylated product formed under an $^{18}O_2$ atmosphere from the hydroxylation substrate, hyoscyamine (showing that the dihydroxylated can incorporate up to two atoms from O_2), and from the 6-OH-Hyo substrate for both wt *Ab*H6H and the L289F variant. For the lowest set of traces, the final concentrations were 0.12 mM *Ab*H6H, 0.1 mM Fe, 0.1 mM Hyo, 0.3 mM 2OG, and 0.9 mM $^{18}O_2$. For the middle set of traces, the final concentrations were 0.12 mM *Ab*H6H, 0.1 mM Fe, 0.1 mM 6-OH-Hyo, 0.3 mM 2OG, and 0.9 mM $^{18}O_2$. For the upper set of traces, the final concentrations were 0.12 mM L289F *Ab*H6H, 0.1 mM Fe, 0.1 mM 6-OH-Hyo, 0.3 mM 2OG, and 0.9 mM $^{18}O_2$. The reactions were carried out in sealed vials within an

anoxic chamber. After initiation by simultaneous addition of 2OG and $^{18}O_2$, reactions were allowed to proceed for 15 min at 25 ºC.

In our previous study involving *Hn*H6H, we showed that out-of-order C7 hydroxylation incorporates ^{18}O from $^{18}O_2$ to a lesser extent than does in-sequence C6 hydroxylation, despite the fact that the two sites of Hyo compete to donate their hydrogens to a common ferryl intermediate.[43] We explained this phenomenon in terms of greater solvent exchange of the oxo-derived hydroxo ligand in the Fe^{III}–OH/C7• intermediate state than in the Fe^{III}–OH/C6• intermediate state, which we attributed to a geometric programming of slower oxygen rebound after HAT from C7.[43] To assess whether the 60-fold enhanced hydroxylation of C7 of 6-OH-Hyo by the L289F variant of *Ab*H6H might result from accelerated oxygen rebound caused by a perturbation in the disposition of the C7• to the Fe(III)–OH cofactor, we compared the extents of ^{18}O incorporation from $^{18}O_2$ into the 6,7-$(OH)_2$-Hyo product formed by the wt and variant *Ab*H6H enzymes. In reactions under $^{18}O_2$, we found only 13% ^{18}O in the dihydroxylated product formed from 6-OH-Hyo by the wt enzyme, consistent with extensive washout in the ferryl intermediate state, the Fe^{III}–OH/C7• state, or both (**Figure 10**). By contrast, we measured 42% ^{18}O incorporation from $^{18}O_2$ in the predominant 6,7-$(OH)_2$-Hyo product produced by the L289F variant in its second reaction. The enhancement of ^{18}O incorporation implies a decreased lifetime of the ferryl or Fe^{III}–OH/C7• intermediate (or both) in the variant. Thus, it appears that, rather than intrinsically disabling epoxidation, the L289F substitution may actually favor oxygen rebound within the Fe^{III}–OH/C7• intermediate. Again, the corollary is that wt H6H somehow actively impedes an intrinsically favorable (or at least eminently possible) rebound step.

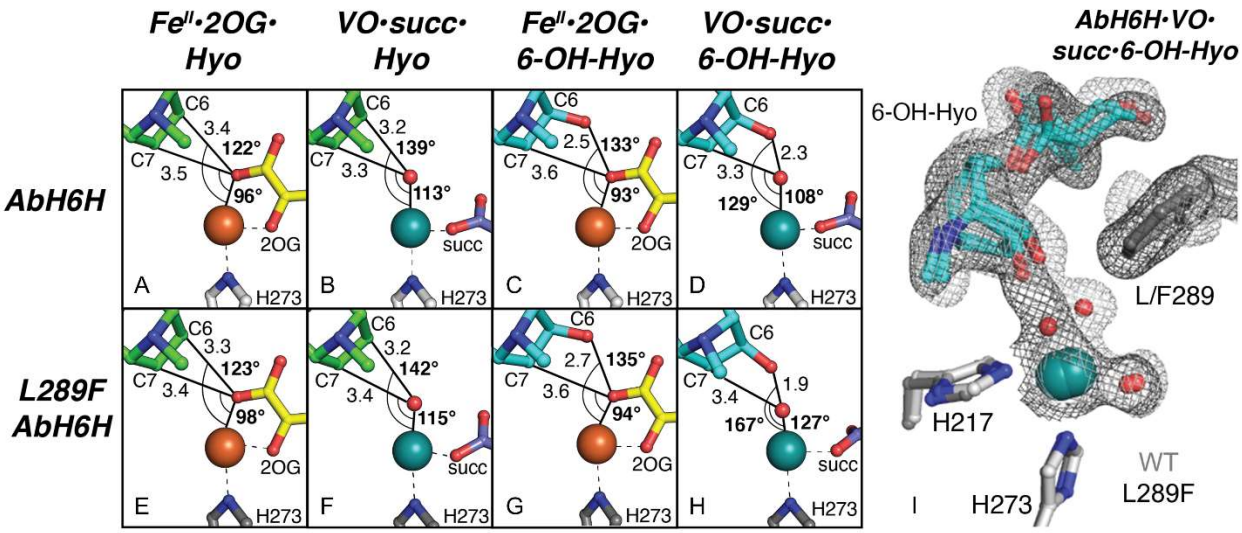

Figure 11. Comparisons of metal-substrate dispositions in each of the four cognate pairs of wt and L289F *Ab*H6H crystal structures. Three of the four pairs overlay within error (compare ***A-C*** to ***E-G***, respectively); only the structures derived from the $V^{IV}O$•succ•6-OH-Hyo complexes reveal a shift resulting from the increased steric bulk in the active site (compare ***D*** to ***H***). (***I***) These structures are overlaid with gray mesh that illustrates $2F_o$-F_c electron density (contoured at 1σ) for the 6-OH-Hyo substrate, the metal and oxygen ligands, and the L289 and F289 sidechains. The lighter mesh corresponds to the wt protein and the darker mesh to the L289F protein. Selected side chains, water molecules, cofactors, and substrates are shown in ball-and-stick or sphere representation and colored according to atom type.

To understand the structural basis for this rebound suppression by wt *Ab*H6H and its unleashing by the L289F substitution, we solved four structures of the L289F variant from crystals of its Fe^{II}•2OG•(6-OH-)Hyo and $V^{IV}O$•succ•(6-OH-)Hyo complexes ranging in resolution from 1.53-2.03 Å (**Figure S30**; statistics shown in **Table S9**). Even though L289 lines the prime substrate binding pocket (**Figure S28**), its substitution by the bulkier F barely perturbs the structure of the Hyo reactant complex and has no obviously significant impact on the configuration of the active site (**Figure 11**, compare **A** to **E**). The minimal structural impact comports with the minor

effect of the substitution on the distribution of products generated from Hyo. Two of the three remaining pairwise comparisons – between the structures derived from the $V^{IV}O$•succ•Hyo and Fe^{II}•2OG•6-OH-Hyo complexes of the wt and L289F proteins – reveal similarly modest changes (**Figure 11**, compare **B** to **F** and **C** to **G**). Among the four pairwise comparisons, only the structures derived from the $V^{IV}O$•succ•6-OH-Hyo complexes reveal a significant change near the cofactor associated with the L289F substitution (**Figure 11**, compare **D** to **H**). The additional bulk of the F residue directly impacts the interaction between the in-line (oxo-derived) oxygen ligand and the substrate C6 hydroxyl. The in-line oxygen shifts to form a 106° O–V–O angle with the off-line (solvent-derived) oxygen ligand, increased by ~ 20° from the angle in the corresponding structure of wt *Ab*H6H. The 6-OH-Hyo substrate shifts to preserve the interaction of the C6-OH group with the in-line ligand. A superposition of the modeled atoms and associated electron density maps for the two proteins illustrates the modest global shift of the 6-OH-Hyo prime substrate (**Figure 11I**, *far right*).

Notably, although the C7–V distances are identical (within error) in the wt and variant structures, the V–O–C7 angle in the L289F variant (127°) is ~ 20° larger than the corresponding angle in wt *Ab*H6H (108°) (**Figure 11**). The perturbation brings this angle closer to those seen in vanadyl-derived structures of the Fe/2OG hydroxylases TauD, VioC, and CAS (132-136°), in which both the initiating HAT and terminating oxygen-rebound steps are relatively efficient (**Table 2**, **Figure 8** and **S26**).[10,44,53] As such, the observed increase in the V–O–C7 angle in the L289F variant offers a rationale for both its diminished capacity for C7–O(C6) coupling (epoxidation) and the diminished fraction of solvent exchange of the initially O_2-derived oxo group during its C7 hydroxylation, with which epoxidation competes. This explanation underscores the

importance of the precise positioning of the substrate tropane core seen in the wt enzyme in enabling the two-step reaction sequence.

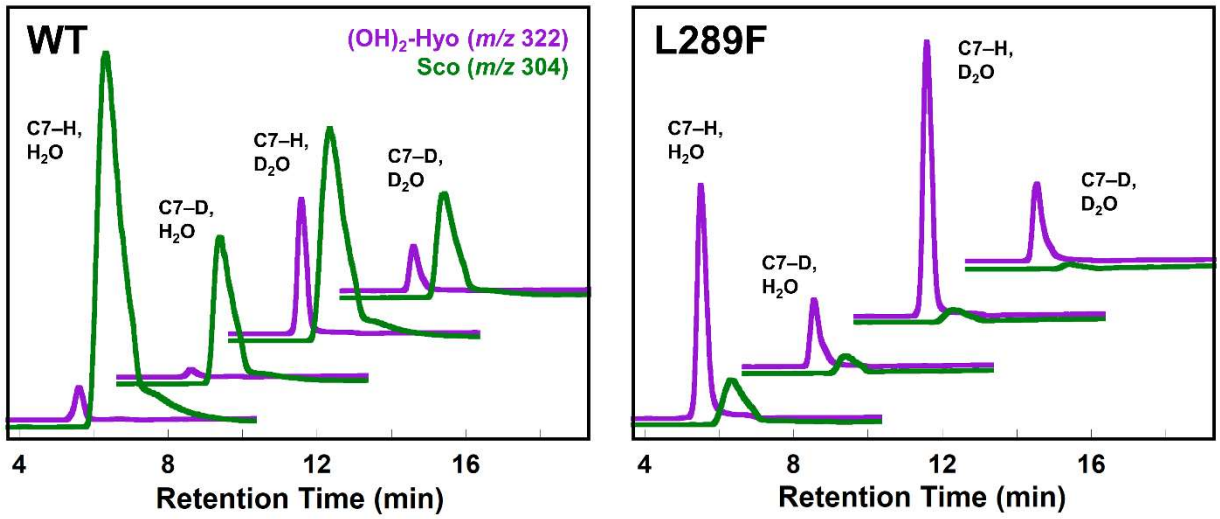

Figure 12. Chromatograms showing the product distributions in reactions of (***A***) wt *Ab*H6H and (***B***) the L289F variant with 6-OH-Hyo and 7-d_1-6-OH-Hyo in H_2O and D_2O. The final concentrations were 0.25 mM *Ab*H6H (L289F or wt), 0.2 mM Fe, 0.5 mM prime substrate, and 0.1 mM 2OG. Assays were allowed to proceed open to atmosphere at 4 °C for 1 h. Product percentages derived from peak integrations are given in **Table 3**.

Table 3. Relative quantification of the products formed by wt and L289F *Ab*H6H with 6-OH-Hyo and 7-d_1-6-OH-Hyo in H_2O and D_2O.

% $(OH)_2$-Hyo Product[a]	WT H_2O	WT D_2O	L289F H_2O	L289F D_2O
6-OH	4.5 ± 0.3	23.7 ± 1.2	74.8 ± 1.4	93.8 ± 0.4
7-d_1-6-OH	3.6 ± 0.3	18.3 ± 0.1	66.5 ± 2.2	91.7 ± 0.4

[a]In each case, the reported value is the percent of the total detected product [Sco + $(OH)_2$-Hyo] that is $(OH)_2$-Hyo. Values in the table were determined as the percentage of the area of each peak to the total area of the two peaks. Each value is an average of three trials.

Solvent deuteration favors rebound over oxacyclization and slows ferryl decay. In addition to cleaving the C7–H bond, H6H must also cleave the (C6)O–H bond of 6-OH-Hyo to promote the epoxidation reaction. Given evidence against coordination of the substrate C6 oxygen to the cofactor, which could theoretically have promoted its deprotonation in advance of C7–H cleavage, we sought to assess the nature and timing of the O–H cleavage step. We reasoned that, because oxygen rebound is not known to require proton transfer, use of D_2O as solvent to replace the protium on the (C6)O–H alcohol might selectively slow epoxide ring closure relative to rebound. Indeed, we determined that the 6,7-$(OH)_2$-Hyo:Sco partition ratio of the reaction of wt *Ab*H6H with 6-OH-Hyo changes from 4:96 in H_2O to 24:76 in D_2O (**Table 3** and **Figure 12**), consistent with a selective slowing (by a factor of ~ 7.6) of the step that commits to the epoxide product in D_2O. Use of D_2O solvent also potentiates the effect of the L289F substitution: in the reaction of the variant protein with 6-OH-Hyo, the $(OH)_2$-Hyo:Sco partition ratio increases from 75:25 in H_2O to 94:6 in D_2O (**Table 3** and **Figure 12**), almost completely inverting the chemoselectivity of wt *Ab*H6H in H_2O.

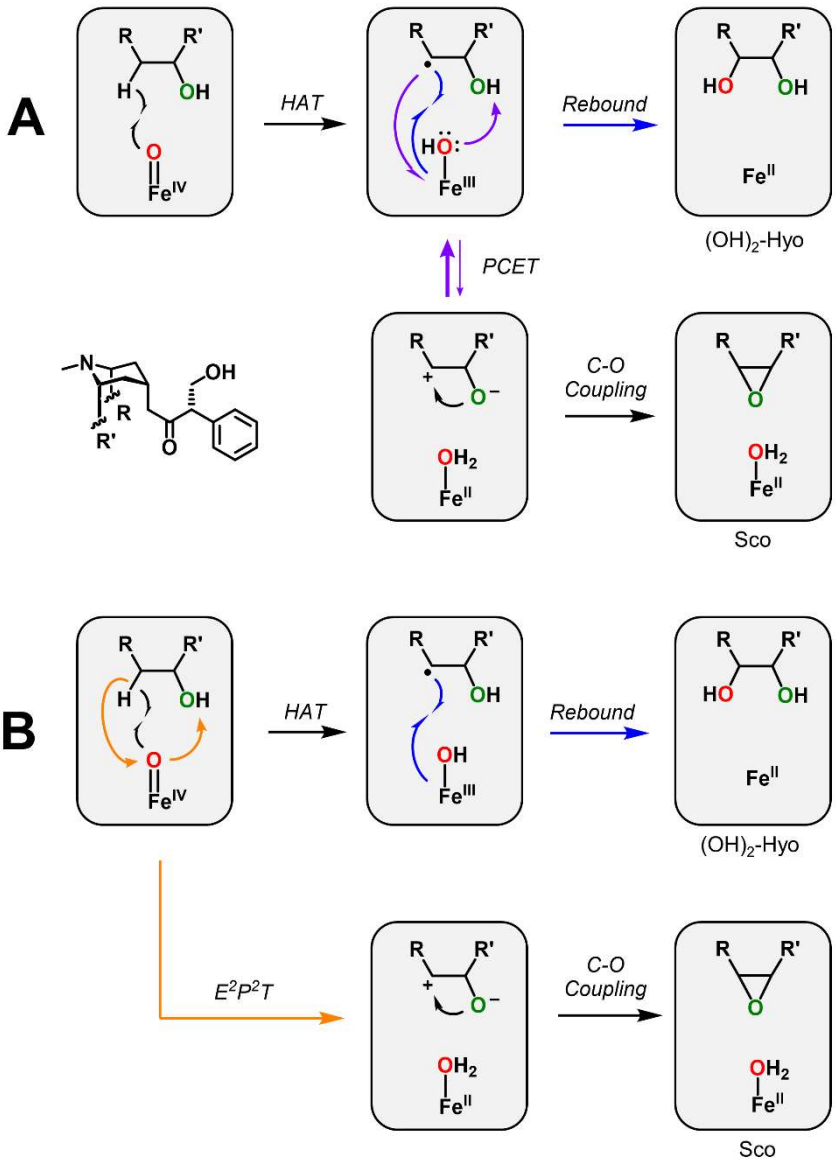

Scheme 3. Possible mechanisms for the H6H-catalyzed epoxidation reaction.

Possible cyclization mechanism accounting for all above data. Along with the structural data, the observed primary substrate C7 D-KIE on decay of the second ferryl intermediate and the primary solvent D-KIE effect on the ratio of 6,7-epoxidation to C7 hydroxylation can be accommodated by the mechanism shown in **Scheme 3A**. A well-precedented HAT to the ferryl complex from C7

of 6-OH-Hyo is followed by reversible electron transfer (ET) from C7 to the Fe(III)–OH cofactor and deprotonation (proton transfer, PT) of the C6 hydroxyl group to prepare the oxygen for coupling to C7 (purple arrows). Given the short (C6)O–O(V) distance seen in the crystal structure, the proton acceptor could be the Fe(III) hydroxo ligand, and this step could be kinetically coupled to, or concerted with, the ET step (PTET, ETPT or PCET). The resultant 1,3-zwitterion would be short-lived, closing rapidly to epoxide. The need for PT in the coupled step that forms this intermediate could explain why, in D_2O, C7 hydroxylation is enhanced: the D-KIE on transfer of the solvent-exchangeable hydron would selectively slow epoxidation relative to C7• oxygen rebound, which is not expected to be subject to a comparable solvent D-KIE.

Test for solvent D-KIE on ferryl decay in H6H epoxidation and other Fe/2OG oxygenase reactions. Because (1) no evidence (of which we are aware) has been presented for reversibility in HAT from carbon to a ferryl complex in an Fe/2OG or related nonheme-iron enzyme and (2), in other enzymes, C–H bonds at least modestly stronger than the methylene exo-C7–H of 6-OH-Hyo are cleaved relatively rapidly and with no indication of reversibility,[29] we assumed that the C7 HAT step in the H6H cyclization reaction would be irreversible. Under this assumption, we reasoned that the solvent D-KIE manifested by the product ratio, which hypothetically arises from C6-OH deprotonation, should not impact the kinetics of decay of the ferryl complex, because HAT to the ferryl complex precedes the PT, and its irreversibility prevents a delay in PT from "feeding back" to delay ferryl decay.

We tested this prediction by SF-Abs experiments in H_2O and D_2O with 6-OH-Hyo and 7-d_1-6-OH-Hyo substrates (**Figure 1**). Surprisingly, we observed a delay in ferryl decay in D_2O for both the natural-abundance and the deuterium-labeled substrate, although the direct kinetic effect

was not as large as the effect on the Sco:6,7-$(OH)_2$-Hyo product ratio. Decay was slowed to 0.35 and 0.06 s^{-1} for the 6-OH-Hyo and 7-d_1-6-OH-Hyo substrates, respectively, for observed solvent D-KIEs of 1.4 for 6-OH-Hyo and 1.8 for 7-d_1-6-OH-Hyo. Because we had not, in our prior work, tested other Fe/2OG enzymes for such an effect, we also evaluated the prototypical hydroxylase, TauD,[62] and the non-native desaturation of deoxyproclavaminate catalyzed by clavaminate synthase[63] to provide examples of different reaction types. By contrast to the case of the H6H epoxidation, we observed no discernable solvent deuterium KIE on ferryl decay in these two reactions (**Figure S31**). More discerningly, as discussed in the preceding paper, we also observed a negligible (perhaps slightly *inverse*) solvent D-KIE on ferryl decay in the LolO oxacyclization reaction, in which we posit that the (C2)OH coordinates to the ferryl species, leading to its deprotonation in advance of HAT and obviating a PT step as part of C7–O(C2) coupling that forms the oxalane ring.[49] The aforementioned mechanism (purple arrows in **Scheme 3A**), which, among the possibilities that we can envisage, aligns most closely with established precedent, does not account for the solvent KIE on ferryl decay seen – uniquely among the four reactions that we tested – in the H6H epoxidation.

In this mechanism, decay of the ferryl complex by HAT from C7 can become kinetically linked with (C6)O–H deprotonation if both the initiating HAT step and the subsequent PT step are reversible and disfavored (scheme at right in **Figure S32**). In this situation, the HAT from C7 will effectively consume the ferryl complex only after the entire three-step sequence is traversed. The large intrinsic D-KIEs associated with hydrogen/proton transfers (which have been explained by the different tunneling efficiencies of protium and deuterium) allow formulation of a set of four rate constants, of which three ($k_{\text{obs H-sub/H2O}}$, $k_{\text{obs D-sub/H2O}}$, $k_{\text{obs H-sub/D2O}}$) are consistent with values determined in this study. Their ratios (which are the observed substrate and solvent D-KIEs) are

also consistent with precedents for such intrinsic D-KIEs. The kinetic scheme that links the C7 HAT and PT steps (at right in **Figure S32**) would imply that the HAT step is endergonic by ~ 1.7 kcal/mol. The likelihood of such an uphill HAT step is difficult to assess. As noted, we are unaware of any experimental evidence for reversibility in HAT from an aliphatic carbon to a ferryl complex, but the absence of such evidence could imply either that the steps immediately following HAT (e.g., oxygen rebound for the hydroxylases) are uniformly much faster than the reverse HAT steps (i.e., a high forward commitment) or that the possibility of reversibility has not been adequately explored. Moreover, DFT and QM-MM studies have not generally agreed as to whether the HAT steps are endergonic or exergonic.[32,64-66]

Despite this uncertainty, the data provide an internal check of the viability of this reversible-HAT scenario to link it to the PT step in the proposed cyclization mechanism. In this case of two different isotopic perturbations (substrate and solvent deuteration) that affect different reaction steps, use of deuterated solvent should diminish the observed substrate D-KIE (*compare red and blue to and orange and purple traces at left in* **Figure S32**), and use of deuterated substrate should diminish the observed solvent D-KIE (*compare red and orange to blue and purple traces at left in* **Figure S32**). As explained by O'Leary,[67] Cleland,[68] Cook,[69] and others in the context of steady-state-kinetic analysis using two isotopic substitutions, slowing one step diminishes the extent to which the other step is rate-limiting for the sequence, and so the intrinsic KIE on the other step becomes less "expressed" in the flux through the multi-step pathway. This predicted co-dependency contrasts starkly with the one shown in **Figure 1**, in which one effect is *potentiated* by the other. In other words, the substrate D-KIE is larger in D_2O than in H_2O (5.8 versus 4.5), and the solvent D-KIE is larger with the deuterium-bearing substrate than with the protium-bearing substrate (1.8 versus 1.4).

In prior studies, observations of this mutual potentiation have been taken as evidence that the two isotopic substitutions affect the *same* reaction step.[67-70] Applying this logic to our results on H6H would imply *concerted* cleavage of C7–H and (C6)O–H bonds in the epoxidation reaction (orange arrows in **Scheme 3B**). A concerted proton-coupled HAT step (H^+ + H•) seems unlikely, as other well-studied cases of neutral hydrogen (H•) transfer are not known to require a PT step, and such a mechanism would result in charge separation. Charge-neutral proton-coupled hydride transfers (H^+ + H^-, denoted PCHT) are known,[71-72] and recent studies have proposed hydride transfers to metal-dioxygen complexes of the sort commonly encountered in reactions involving initiating HAT steps.[73] However, it is difficult to conceive of such a mechanism in this reaction, which would involve transfer of a hydride from a carbon lacking an activating heteroatom to a high-spin (S = 2) ferryl complex. Computational analysis of the feasibility of a mechanism involving such a 2-electron/2-proton transfer (E^2P^2T) to a ferryl complex is perhaps warranted. If such a mechanism could occur, it might recast the demonstrated rigid positioning requirements of the H6H epoxidation in terms of the imperative to suppress the canonical HAT reactivity in favor of the unusual E^2P^2T leading directly to the postulated 1,3-zwitterion that cyclizes to complete the reaction. Competition by HAT, leading to C7 hydroxylation instead of epoxidation (blue arrows in **Scheme 3B**), would be enhanced in D_2O, because only the unusual E^2P^2T step would involve transfer of a solvent exchangeable hydron. Disruption of the special substrate-intermediate disposition by the L289F substitution would allow HAT to outcompete the E^2P^2T, resulting in predominant hydroxylation, especially in D_2O. The likelihood of this alternative explanation is difficult to assess until (and unless) a possible pathway has been identified and its activation barrier(s) evaluated.

Conclusion

The data presented demonstrate that neither coordination of the C6-OH to the iron center nor major reconfiguration of the active site is required for the switch in outcome from C6 hydroxylation in the first reaction to C7–O(C6) coupling in the second reaction of H6H. Instead, the enzyme achieves selective epoxidation by enforcing a possibly unique substrate-binding mode that disfavors oxygen insertion (hydroxylation) and allows a chemically challenging, strain-incorporating, alternative C–O-coupling (epoxidation) step to prevail in the second reaction. Strategic introduction of additional steric bulk in a single residue near the active site tilts the substrate ~ 20° from this special binding mode and unleashes the default oxygen-insertion reactivity of the second ferryl complex, thus largely preempting epoxidation. The least radical interpretation of the data is in terms of a cyclization mechanism involving polar capture of a C7 carbocation – formed in a rapid and disfavored PT-coupled ET to the Fe(III) cofactor after HAT from C7 – by the C6 alkoxide, a mechanism that would align with proposals advanced in recent studies on aziridine formation by Fe/2OG enzymes.[74] The requirement for C6–OH deprotonation to allow for successful capture of the disfavored C7 carbocation would explain the large solvent D-KIE of ~ 8 on the epoxidation:hydroxylation partition ratio. The surprising and – by this mechanism – unexplained observation of a smaller solvent D-KIE also on ferryl decay leaves open the possibility of a more divergent mechanism involving highly coupled or concerted cleavage of the (C6)O–H and C7–H bonds by the second ferryl complex, which would recast the extraordinarily strict geometric requirements of the H6H epoxidation reaction in terms of the need to disfavor the conventional C7-HAT relative to the hypothetical E^2P^2T step. Irrespective of which scenario is operant, the dichotomy between the mechanisms deduced here for H6H and in a parallel study of LolO, in a pair of reactions that are superficially similar, reinforces the previously noted[15]

importance of substrate and product structures in constraining chemical pathways that may be available for enzymatic acceleration of such chemically challenging C–H-functionalization reactions.

Acknowledgements

This work was supported by the National Institutes of Health (GM113106 to J.M.B., Jr. and C.K., GM118812 to J.M.B., Jr., GM 127079 to C.K., GM141284 to A.S., and GM119707 to A.K.B.). R.J.M. acknowledges the support of a National Science Foundation Graduate Research Fellowship. C.J.P. acknowledges support of the National Institute of General Medical Sciences in the National Institute of Health (F32GM113389). This research used LS-CAT and GM/CA-CAT beamlines at the Advanced Photo Source of Argonne National Laboratory and the resources of a U.S. Department of Energy (DOE) Office of Science by Argonne National Laboratory under Contact No. DEAC02-06CH11357.

References

1. Dunham, N. P.; Arnold, F. H., Nature's Machinery, Repurposed: Expanding the Repertoire of Iron-Dependent Oxygenases. *ACS Catalysis* **2020,** *10*, 12239-12255.

2. Cheung-Lee, W. L.; Kolev, J. N.; McIntosh, J. A.; Gil, A. A.; Pan, W.; Xiao, L.; Velásquez, J. E.; Gangam, R.; Winston, M. S.; Li, S.; Abe, K.; Alwedi, E.; Dance, Z. E. X.; Fan, H.; Hiraga, K.; Kim, J.; Kosjek, B.; Le, D. N.; Salehi Marzijarani, N.; Mattern, K.; McMullen, J. P.; Narsimhan, K.; Vikram, A.; Wang, W.; Yan, J.-X.; Yang, R.-S.; Zhang, V.; Zhong, W.; DiRocco, D. A.; Morris, W. J.; Murphy, G. S.; Maloney, K. M., Engineering Hydroxylase Activity, Selectivity, and Stability for a Scalable Concise Synthesis of a Key Intermediate to Belzutifan. *Angewandte Chemie International Edition n/a*, e202316133.

3. Hausinger, R. P., FeII/alpha-ketoglutarate-dependent hydroxylases and related enzymes. *Crit. Rev. Biochem. Mol. Biol.* **2004,** *39*, 21-68.

4. Bollinger, J. M., Jr.; Chang, W.-c.; Matthews, M. L.; Martinie, R. J.; Boal, A. K.; Krebs, C., Mechanisms of 2-Oxoglutarate-Dependent Oxygenases: The Hydroxylation Paradigm and Beyond. In *2-Oxoglutarate-Dependent Oxygenases*, Hausinger, R. P.; Schofield, C. J., Eds. Royal Society of Chemistry: 2015; pp 95-122.

5. Mitchell, A. J.; Dunham, N. P.; Martinie, R. J.; Bergman, J. A.; Pollock, C. J.; Hu, K.; Allen, B. D.; Chang, W.-c.; Silakov, A.; Bollinger, J. M., Jr.; Krebs, C.; Boal, A. K., Visualizing the reaction cycle in an Iron(II)- and 2-(oxo)-glutarate-dependent hydroxylase. *J. Am. Chem. Soc.* **2017,** *139*, 13830-13836.

6. Ye, S. F.; Riplinger, C.; Hansen, A.; Krebs, C.; Bollinger, J. M., Jr.; Neese, F., Electronic structure analysis of the oxygen-activation mechanism by Fe-II- and alpha-ketoglutarate (alpha KG)-dependent dioxygenases. *Chem.: Eur. J.* **2012,** *18*, 6555-6567.

7. Hanauske-Abel, H. M.; Günzler, V., A stereochemical concept for the catalytic mechanism of prolylhydroxylase. Applicability to classification and design of inhibitors. *J. Theor. Biol.* **1982,** *94*, 421-455.

8. Price, J. C.; Barr, E. W.; Glass, T. E.; Krebs, C.; Bollinger Jr., J. M., Evidence for hydrogen abstraction from C1 of taurine by the high-spin Fe(IV) intermediate detected during oxygen activation by taurine:α-ketoglutarate dioxygenase (TauD). *J. Am. Chem. Soc.* **2003,** *125*, 13008-13009.

9. Price, J. C.; Barr, E. W.; Tirupati, B.; Bollinger, J. M., Jr.; Krebs, C., The first direct characterization of a high-valent iron intermediate in the reaction of an a-ketoglutarate-dependent dioxygenase: A high-spin Fe(IV) complex in taurine/a-ketoglutarate dioxygenase (TauD) from *Escherichia coli*. *Biochemistry* **2003,** *42*, 7497-7508.

10. Price, J. C.; Barr, E. W.; Hoffart, L. M.; Krebs, C.; Bollinger, J. M., Jr., Kinetic dissection of the catalytic mechanism of taurine:α-ketoglutarate dioxygenase (TauD) from *Escherichia coli*. *Biochemistry* **2005,** *44*, 8138-8147.

11. Ho, R. Y. N.; Mehn, M. P.; Hegg, E. L.; Liu, A.; Ryle, M. J.; Hausinger, R. P.; Que, L., Jr., Resonance Raman studies of the iron(II)-a-keto acid chromophore in model and enzyme complexes. *J. Am. Chem. Soc.* **2001,** *123*, 5022-5029.

12. Hoffart, L. M.; Barr, E. W.; Guyer, R. B.; Bollinger, J. M., Jr.; Krebs, C., Direct spectroscopic detection of a C–H-cleaving high-spin Fe(IV) complex in a prolyl-4-hydroxylase. *Proc. Natl. Acad. Sci. U.S.A.* **2006,** *103*, 14738-14743.

13. Groves, J. T., Key elements of the chemistry of cytochrome P-450: the oxygen rebound mechanism. *J. Chem. Educ.* **1985,** *62*, 928-931.

14. Vaillancourt, F. H.; Yin, J.; Walsh, C. T., SyrB2 in syringomycin E biosynthesis is a nonheme FeII α-ketoglutarate- and O2-dependent halogenase. *Proc. Natl. Acad. Sci. U.S.A.* **2005,** *102*, 10111-10116.

15. Dunham, N. P.; Chang, W.-c.; Mitchell, A. J.; Martinie, R. J.; Zhang, B.; Bergman, J. A.; Rajakovich, L. J.; Wang, B.; Silakov, A.; Krebs, C.; Boal, A. K.; Bollinger, J. M., Jr., Two distinct mechanisms for C–C desaturation by iron(II)- and 2-(oxo)glutarate-dependent oxygenases: importance of α-heteroatom assistance. *J. Am. Chem. Soc.* **2018,** *140*, 7116-7126.

16. Pan, J.; Bhardwaj, M.; Zhang, B.; Chang, W.-c.; Schardl, C. L.; Krebs, C.; Grossman, R. B.; Bollinger, J. M., Jr., Installation of the ether bridge of lolines by the iron- and 2-oxoglutarate-dependent oxygenase, LolO: regio- and stereochemistry of sequential hydroxylation and oxacyclization reactions. *Biochemistry* **2018,** *57*, 2074-2083.

17. Lee, H.-J.; Lloyd, M. D.; Harlos, K.; Clifton, I. J.; Baldwin, J. E.; Schofield, C. J., Kinetic and crystallographic studies on deacetoxycephalosporin C synthase (DAOCS). *J. Mol. Biol.* **2001,** *308*, 937-948.

18. Chang, W.-c.; Guo, Y.; Wang, C.; Butch, S. E.; Rosenzweig, A. C.; Boal, A. K.; Krebs, C.; Bollinger, J. M., Jr., Mechanism of the C5 stereoinversion reaction in the biosynthesis of carbapenem antibiotics. *Science* **2014,** *343*, 1140-1144.

19. Marchand, J. A.; Neugebauer, M. E.; Ing, M. C.; Lin, C. I.; Pelton, J. G.; Chang, M. C. Y., Discovery of a pathway for terminal-alkyne amino acid biosynthesis. *Nature* **2019,** *567*, 420-424.

20. Hillwig, M. L.; Liu, X., A new family of iron-dependent halogenases acts on freestanding substrates. *Nature Chem. Biol.* **2014,** *10*, 921-923.

21. Ishikawa, N.; Tanaka, H.; Koyama, F.; Noguchi, H.; Wang, C. C. C.; Hotta, K.; Watanabe, K., Non-Heme Dioxygenase Catalyzes Atypical Oxidations of 6,7-Bicyclic Systems To Form the

6,6-Quinolone Core of Viridicatin-Type Fungal Alkaloids. *Angewandte Chemie International Edition* **2014,** *53*, 12880-12884.

22. Gama, S. R.; Stankovic, T.; Hupp, K.; Al Hejami, A.; McClean, M.; Evans, A.; Beauchemin, D.; Hammerschmidt, F.; Pallitsch, K.; Zechel, D. L., Biosynthesis of the Fungal Organophosphonate Fosfonochlorin Involves an Iron(II) and 2-(Oxo)glutarate Dependent Oxacyclase. *Chembiochem* **2022,** *23*, e202100352.

23. Hashimoto, T.; Matsuda, J.; Yamada, Y., 2-Step epoxidation of hyoscyamine to scopolamine is catalyzed by bifunctional hyscyamine 6-beta-hydroxylase. *FEBS Lett.* **1993,** *329*, 35-39.

24. Blasiak, L. C.; Vaillancourt, F. H.; Walsh, C. T.; Drennan, C. L., Crystal structure of the non-haem iron halogenase SyrB2 in syringomycin biosynthesis. *Nature* **2006,** *440*, 368-371.

25. Koehntop, K. D.; Emerson, J. P.; Que, L., Jr., The 2-His-1-carboxylate facial triad: A versatile platform for dioxygen activation by mononuclear non-heme iron(II) enzymes. *J. Biol. Inorg. Chem.* **2005,** *10*, 87-93.

26. Galonić Fujimori, D.; Barr, E. W.; Matthews, M. L.; Koch, G. M.; Yonce, J. R.; Walsh, C. T.; Bollinger, J. M., Jr.; Krebs, C.; Riggs-Gelasco, P. J., Spectroscopic evidence for a high-spin Br-Fe(IV)-oxo intermediate in the a-ketoglutarate-dependent halogenase CytC3 from *Streptomyces*. *J. Am. Chem. Soc.* **2007,** *129*, 13408-13409.

27. Galonić, D. P.; Barr, E. W.; Walsh, C. T.; Bollinger, J. M., Jr.; Krebs, C., Two interconverting Fe(IV) intermediates in aliphatic chlorination by the halogenase CytC3. *Nature Chem. Biol.* **2007,** *3*, 113-116.

28. Matthews, M. L.; Krest, C. M.; Barr, E. W.; Vaillancourt, F. H.; Walsh, C. T.; Green, M. T.; Krebs, C.; Bollinger, J. M., Jr., Substrate-triggered formation and remarkable stability of the

C–H bond-cleaving chloroferryl intermediate in the aliphatic halogenase, SyrB2. *Biochemistry* **2009,** *48*, 4331-4343.

29. Matthews, M. L.; Neumann, C. S.; Miles, L. A.; Grove, T. L.; Booker, S. J.; Krebs, C.; Walsh, C. T.; Bollinger, J. M., Jr., Substrate positioning controls the partition between halogenation and hydroxylation in the aliphatic halogenase, SyrB2. *Proc. Natl. Acad. Sci. U.S.A.* **2009,** *106*, 17723-17728.

30. Martinie, R. J.; Livada, J.; Chang, W.-c.; Green, M. T.; Krebs, C.; Bollinger, J. M., Jr.; Silakov, A., Experimental correlation of substrate position with reaction outcome in the aliphatic halogenase, SyrB2. *J. Am. Chem. Soc.* **2015,** *137*, 6912-6919.

31. Srnec, M.; Solomon, E. I., Frontier molecular orbital contributions to chlorination versus hydroxylation selectivity in the non-heme iron halogenase SyrB2. *J. Am. Chem. Soc.* **2017,** *139*, 2396-2407.

32. Wong, S. D.; Srnec, M.; Matthews, M. L.; Liu, L. V.; Kwak, Y.; Park, K.; Bell, C. B.; Alp, E. E.; Zhao, J. Y.; Yoda, Y.; Kitao, S.; Seto, M.; Krebs, C.; Bollinger, J. M., Jr.; Solomon, E. I., Elucidation of the Fe(IV)=O intermediate in the catalytic cycle of the halogenase SyrB2. *Nature* **2013,** *499*, 320-323.

33. Hausinger, R. P., Fe(II)/α-ketoglutarate-dependent hydroxylases and related enzymes. *Crit. Rev. Biochem. Mol. Biol.* **2004,** *39*, 21-68.

34. Zhang, Z. H.; Ren, J. S.; Harlos, K.; McKinnon, C. H.; Clifton, I. J.; Schofield, C. J., Crystal structure of a clavaminate synthase-Fe(II)-2-oxoglutarate-substrate-NO complex: evidence for metal centred rearrangements. *FEBS Lett.* **2002,** *517*, 7-12.

35. Mitchell, A. J.; Zhu, Q.; Maggiolo, A. O.; Ananth, N. R.; Hillwig, M. L.; Liu, X. Y.; Boal, A. K., Structural basis for halogenation by iron- and 2-oxo-glutarate-dependent enzyme WelO5. *Nature chemical biology* **2016,** *12*, 636-640.

36. Vennelakanti, V.; Mehmood, R.; Kulik, H. J., Are Vanadium Intermediates Suitable Mimics in Non-Heme Iron Enzymes? An Electronic Structure Analysis. *ACS Catalysis* **2022,** *12*, 5489-5501.

37. Kastner, D. W.; Nandy, A.; Mehmood, R.; Kulik, H. J., Mechanistic Insights into Substrate Positioning That Distinguish Non-heme Fe(II)/α-Ketoglutarate-Dependent Halogenases and Hydroxylases. *ACS Catalysis* **2023,** *13*, 2489-2501.

38. Pan, J.; Bhardwaj, M.; Faulkner, J. R.; Nagabhyru, P.; Charlton, N. D.; Higashi, R. M.; Miller, A.-F.; Young, C. A.; Grossman, R. B.; Schardl, C. L., Ether bridge formation in loline alkaloid biosynthesis. *Phytochemistry* **2014,** *98*, 60-68.

39. Busby, R. W.; Townsend, C. A., A single monomeric iron center in clavaminate synthase catalyzes three nonsuccessive oxidative transformations. *Bioorganic & Medicinal Chemistry* **1996,** *4*, 1059-1064.

40. Salowe, S. P.; Marsh, E. N.; Townsend, C. A., Purification and characterization of clavaminate synthase from Streptomyces clavuligerus: an unusual oxidative enzyme in natural product biosynthesis. *Biochemistry* **1990,** *29*, 6499-6508.

41. Li, J.; van Belkum, M. J.; Vederas, J. C., Functional characterization of recombinant hyoscyamine 6 beta-hydroxylase from *Atropa belladonna*. *Bioorg. Med. Chem.* **2012,** *20*, 4356-4363.

42. Ushimaru, R.; Ruszczycky, M. W.; Liu, H.-w., Changes in regioselectivity of H atom abstraction during the hydroxylation and cyclization reactions catalyzed by hyoscyamine 6*β*-hydroxylase. *J. Am. Chem. Soc.* **2019,** *141*, 1062-1066.

43. Pan, J.; Wenger, E. S.; Matthews, M. L.; Pollock, C. J.; Bhardwaj, M.; Kim, A. J.; Allen, B. D.; Grossman, R. B.; Krebs, C.; Bollinger Jr., J. M., Evidence for modulation of oxygen rebound rate in control of outcome by iron(II)- and 2-oxoglutarate-dependent oxygenases. *J. Am. Chem. Soc.* **2019,** *141*, 15153-15165.

44. Dunham, N. P.; Mitchell, A. J.; Del Río Pantoja, J. M.; Krebs, C.; Bollinger, J. M., Jr.; Boal, A. K., α-Amine desaturation of D-arginine by the iron(II)- and 2-(oxo)glutarate-dependent L-arginine 3-hydroxylase, VioC. *Biochemistry* **2018,** *57*, 6479-6488.

45. Copeland, R. A.; Davis, K. M.; Shoda, T. K. C.; Blaesi, E. J.; Boal, A. K.; Krebs, C.; Bollinger, J. M., Jr., An Iron(IV)–Oxo Intermediate Initiating L-Arginine Oxidation but Not Ethylene Production by the 2-Oxoglutarate-Dependent Oxygenase, Ethylene-Forming Enzyme. *J. Am. Chem. Soc.* **2021,** *143*, 2293-2303.

46. Pan, J.; Wenger, E. S.; Matthews, M. L.; Pollock, C. J.; Bhardwaj, M.; Kim, A. J.; Allen, B. D.; Grossman, R. B.; Krebs, C.; Bollinger, J. M., Jr., Evidence for Modulation of Oxygen Rebound Rate in Control of Outcome by Iron(II)- and 2-Oxoglutarate-Dependent Oxygenases. *J. Am. Chem. Soc.* **2019,** *141*, 15153-15165.

47. Dassama, L. M. K.; Yosca, T. H.; Conner, D. A.; Lee, M. H.; Blanc, B.; Streit, B. R.; Green, M. T.; DuBois, J. L.; Krebs, C.; Bollinger, J. M., Jr., O_2-Evolving Chlorite Dismutase as a Tool for Studying O_2-Utilizing Enzymes. *Biochemistry* **2012,** *51*, 1607-1616.

48. Krebs, C.; Dassama, L. M. K.; Matthews, M. L.; Jiang, W.; Price, J. C.; Korboukh, V.; Li, N.; Bollinger, J. M., Jr., Novel approaches for the accumulation of oxygenated intermediates to multi-millimolar concentrations. *Coord. Chem. Rev.* **2013,** *257*, 234-243.

49. Pan, J.; Wenger, E. S.; Sil, D.; Zhang, B.; Schaperdoth, I.; Saryazdi, S.; Grossman, R. B.; Bollinger, J. M., Jr.; Krebs, C., An Unusual Ferryl Intermediate and its Implications for the Mechanism of Oxolane Ring Closure by the Loline-Forming Iron(II)- and 2-Oxoglutarate-Dependent Oxygenase, LolO. **2024**.

50. Kluza, A.; Wojdyla, Z.; Mrugala, B.; Kurpiewska, K.; Porebski, P. J.; Niedzialkowska, E.; Minor, W.; Weiss, M. S.; Borowski, T., Regioselectivity of hyoscyamine 6β-hydroxylase-catalysed hydroxylation as revealed by high-resolution structural information and QM/MM calculations. *Dalton Transactions* **2020,** *49*, 4454-4469.

51. Li, J.; Liao, H.-J.; Tang, Y.; Huang, J.-L.; Cha, L.; Lin, T.-S.; Lee, J. L.; Kurnikov, I. V.; Kurnikova, M. G.; Chang, W.-c.; Chan, N.-L.; Guo, Y., Epoxidation Catalyzed by the Nonheme Iron(II)- and 2-Oxoglutarate-Dependent Oxygenase, AsqJ: Mechanistic Elucidation of Oxygen Atom Transfer by a Ferryl Intermediate. *J. Am. Chem. Soc.* **2020,** *142*, 6268-6284.

52. Martinie, R. J.; Pollock, C. J.; Matthews, M. L.; Bollinger, J. M., Jr.; Krebs, C.; Silakov, A., Vanadyl as a Stable Structural Mimic of Reactive Ferryl Intermediates in Mononuclear Nonheme-Iron Enzymes. *Inorganic Chemistry* **2017,** *56*, 13382-13389.

53. Davis, K. M.; Altmyer, M.; Martinie, R. J.; Schaperdoth, I.; Krebs, C.; Bollinger, J. M., Jr.; Boal, A. K., Structure of a Ferryl Mimic in the Archetypal Iron(II)- and 2-(Oxo)-glutarate-Dependent Dioxygenase, TauD. *Biochemistry* **2019,** *58*, 4218-4223.

54. Jonnalagadda, R.; Del Rio Flores, A.; Cai, W.; Mehmood, R.; Narayanamoorthy, M.; Ren, C.; Zaragoza, J. P. T.; Kulik, H. J.; Zhang, W.; Drennan, C. L., Biochemical and crystallographic

investigations into isonitrile formation by a nonheme iron-dependent oxidase/decarboxylase. *Journal of Biological Chemistry* **2021,** *296*, 100231.

55. Vennelakanti, V.; Jeon, M.; Kulik, H., How Do Differences in Electronic Structure Affect the Use of Vanadium Intermediates as Mimics in Non-heme Iron Hydroxylases? *ChemRxiv* **2023**.

56. Vavra, J., Dunham, N. P., Krebs, C., Boal, A. K., Bollinger, J. M. Jr., X-ray crystal structure of clavaminate synthase with vanadyl, succinate, and deoxyproclavaminic acid. *PDB ID 6VWQ* **2021**.

57. Wu, L.; Wang, Z.; Cen, Y.; Wang, B.; Zhou, J., Structural Insight into the Catalytic Mechanism of the Endoperoxide Synthase FtmOx1. *Angewandte Chemie International Edition* **2022,** *61*, e202112063.

58. Geng, C.; Ye, S.; Neese, F., Analysis of Reaction Channels for Alkane Hydroxylation by Nonheme Iron(IV)–Oxo Complexes. *Angewandte Chemie International Edition* **2010,** *49*, 5717-5720.

59. Riggs-Gelasco, P. J.; Price, J. C.; Guyer, R. B.; Brehm, J. H.; Barr, E. W.; Bollinger, J. M., Jr.; Krebs, C., EXAFS spectroscopic evidence for an Fe=O unit in the Fe(IV) intermediate observed during oxygen activation by taurine:a-ketoglutarate dioxygenase. *J. Am. Chem. Soc.* **2004,** *126*, 8108-8109.

60. Baldwin, J. E.; Bradley, M., Isopenicillin *N* synthase: Mechanistic studies. *Chem. Rev.* **1990,** *90*, 1079-1088.

61. Ushimaru, R.; Ruszczycky, M. W.; Chang, W.-c.; Yan, F.; Liu, Y.-n.; Liu, H.-w., Substrate conformation correlates with the outcome of hyoscyamine 6*β*-hydroxylase catalyzed oxidation reactions. *J. Am. Chem. Soc.* **2018,** *140*, 7433-7436.

62. Bollinger, J. M., Jr.; Price, J. C.; Hoffart, L. M.; Barr, E. W.; Krebs, C., Mechanism of Taurine: α-Ketoglutarate Dioxygenase (TauD) from *Escherichia coli*. **2005,** *2005*, 4245-4254.

63. Zhou, J.; Kelly, W. L.; Bachmann, B. O.; Gunsior, M.; Townsend, C. A.; Solomon, E. I., Spectroscopic Studies of Substrate Interactions with Clavaminate Synthase 2, a Multifunctional α-KG-Dependent Non-Heme Iron Enzyme: Correlation with Mechanisms and Reactivities. *J. Am. Chem. Soc.* **2001,** *123*, 7388-7398.

64. Ye, S.; Neese, F., Nonheme oxo-iron(IV) intermediates form an oxyl radical upon approaching the C–H bond activation transition state. *Proc. Natl. Acad. Sci. U. S. A.* **2010,** *108*, 1228-1233.

65. Borowski, T.; Noack, H.; Radoń, M.; Zych, K.; Siegbahn, P. E. M., Mechanism of Selective Halogenation by SyrB2: A Computational Study. *J. Am. Chem. Soc.* **2010,** *132*, 12887-12898.

66. de Visser, S. P., Trends in Substrate Hydroxylation Reactions by Heme and Nonheme Iron(IV)-Oxo Oxidants Give Correlations between Intrinsic Properties of the Oxidant with Barrier Height. *J. Am. Chem. Soc.* **2010,** *132*, 1087-1097.

67. O'Leary, M. H., Multiple Isotope Effects On Enzyme-Catalyzed Reactions. *Annual Review of Biochemistry* **1989,** *58*, 377-401.

68. Cleland, W. W., The use of isotope effects to determine enzyme mechanisms. *Arch. Biochem. Biophys.* **2005,** *433*, 2-12.

69. Cook, P. F., Mechanism from isotope effects. *Isot. Environ. Health Stud.* **1997,** *33*, 3-17.

70. Hermes, J. D.; Tipton, P. A.; Fisher, M. A.; O'Leary, M. H.; Morrison, J. F.; Cleland, W. W., Mechanisms of enzymatic and acid-catalyzed decarboxylations of prephenate. *Biochemistry* **1984,** *23*, 6263-6275.

71. Devi, T.; Lee, Y.-M.; Fukuzumi, S.; Nam, W., Acid-promoted hydride transfer from an NADH analogue to a Cr(III)–superoxo complex via a proton-coupled hydrogen atom transfer. *Dalton Transactions* **2021,** *50*, 675-680.

72. Karton, A.; Greatrex, B. W.; O'Reilly, R. J., Intramolecular Proton-Coupled Hydride Transfers with Relatively Low Activation Barriers. *J. Phys. Chem.* **2023,** *127*, 5713-5722.

73. Zhu, W.; Wu, P.; Larson, V. A.; Kumar, A.; Li, X.-X.; Seo, M. S.; Lee, Y.-M.; Wang, B.; Lehnert, N.; Nam, W., Electronic Structure and Reactivity of Mononuclear Nonheme Iron–Peroxo Complexes as a Biomimetic Model of Rieske Oxygenases: Ring Size Effects of Macrocyclic Ligands. *J. Am. Chem. Soc.* **2024,** *146*, 250-262.

74. Cha, L.; Paris, J. C.; Zanella, B.; Spletzer, M.; Yao, A.; Guo, Y.; Chang, W.-c., Mechanistic Studies of Aziridine Formation Catalyzed by Mononuclear Non-Heme Iron Enzymes. *J. Am. Chem. Soc.* **2023,** *145*, 6240-6246.